Lithos 106 (2008) 365–379

Contents lists available at ScienceDirect

Lithos

journal homepage: www.elsevier.com/locate/lithos

U–Pb zircon age, geochemical and Sr–Nd–Pb–Hf isotopic constraints on age and origin of alkaline intrusions and associated mafic dikes from Sulu orogenic belt, Eastern China

Shen Liu [a,b,*], Ruizhong Hu [b], Shan Gao [a], Caixia Feng [b], Youqiang Qi [b], Tao Wang [b], Guangying Feng [b], Ian M. Coulson [c]

[a] State Key Laboratory of Ore Deposit Geochemistry, Institute of Geochemistry, Chinese Academy of Sciences, Guiyang 550002, China
[b] State Key Laboratory of Geological Processes and Mineral Resources, China University of Geosciences, Wuhan 430074, China
[c] Solid Earth Studies Laboratory, Department of Geology, University of Regina, Regina. Saskatchewan, Canada S4S 0A2

ARTICLE INFO

Article history:
Received 21 May 2008
Accepted 4 September 2008
Available online 24 September 2008

Keywords:
Post-orogenic magmatic activities
Alkaline association
Foundering
Sulu belt
Eastern China

ABSTRACT

Post-orogenic alkaline intrusions and associated mafic dikes from the Sulu orogenic belt of eastern China consist of quartz monzonites, A-type granites and associated mafic dikes. We report here U–Pb zircon ages, geochemical data and Sr–Nd–Pb–Hf isotopic data for these rocks. The SHRIMP U–Pb zircon analyses yield consistent ages ranging from 120.3±2.1 Ma to 126.9±1.9 Ma for five samples from the felsic rocks, and two crystallization ages of 119.0±1.7 Ma and 120.2±1.9 Ma for the mafic dikes. The felsic rocks and mafic dikes are characterized by high $(^{87}Sr/^{86}Sr)_i$ ranging from 0.7079 to 0.7089, low $\varepsilon_{Nd}(t)$ values from −15.3 to −19.2, $^{206}Pb/^{204}Pb$=16.54–17.25, $^{207}Pb/^{204}Pb$=15.38–15.63, $^{208}Pb/^{204}Pb$=37.15–38.45, and relatively uniform $\varepsilon_{Hf}(t)$ values of between −21.6±0.6 and −23.7±1.0, for the magmatic zircons. The results suggest that they were derived from a common enriched lithospheric mantle source that was metasomatized by foundered lower crustal eclogitic materials before magma generation. Geochemical and isotopic characteristics imply that the primary magma to these rocks originated through partial melting of ancient lithospheric mantle that was variably hybridized by melts derived from foundered lower crustal eclogite. The mafic dikes may have been generated by subsequent fractionation of clinopyroxene, whereas the felsic rocks resulted from fractionation of potassium feldspar, plagioclase and ilmenite or rutile. Both were not affected by crustal contamination. Combined with previous studies, these findings provide new evidence that the intense lithospheric thinning beneath the Sulu belt of eastern China occurred between 119 and 127 Ma, and that this was caused by the removal of the lower lithosphere (mantle and lower crust).

1. Introduction

The Sulu high pressure (HP) to ultra-high pressure (UHP) metamorphic belt is widely accepted as the eastern part of Qinling–Dabie collisional orogenic belt between the North China and Yangtze Blocks (e.g., Yin and Ni, 1993; Xu and Zhu, 1994; Cong, 1996; Ye et al., 1996; Jahn et al., 1996; Li et al., 1999; Ye et al., 2000; Zheng et al., 2002), where HP–UHP metamorphic rocks, such as at Rizhao, Qingdao and Weihai (Ye et al., 1996; Cong, 1996; Jahn et al., 1996; Zheng et al., 2003) and voluminous syn-collisional and post-collisional magmatic rocks, such as alkaline complexes (Chen et al., 2003; Guo et al., 2005; Yang et al., 2005a,b), volcanic rocks (Fan et al., 2001; Guo et al., 2004), granitoids and diorite (Zhao et al., 1997; Zhou and Lu, 2000; Hong et al., 2003; Huang et al., 2005; Yang et al., 2005a,b), gabbro (Meng et al., 2005), mafic dikes (Guo et al., 2004; Yang et al., 2005a,b) and adakites (Guo et al., 2006) are widespread. These rocks contain valuable information about deep dynamic processes, and can be used to study the orogenic processes of continental subduction and the role of crust–mantle interaction (Menzies and Kyle, 1990; Jahn et al., 1996; Ye et al., 2000; Fan et al., 2001; Guo et al., 2004).

It is generally believed that alkaline rocks mostly come from the upper mantle (Ren, 2003), and are emplaced in non-orogenic, intraplate extensional and/or rift-related tectonic settings (Currie, 1970; Yan et al., 2002). However, alkaline rocks may be emplaced in post-orogenic stages in a short interval of time, such as the Permian–Triassic Western Mediterranean province (Bonin et al., 1987), the Pan-African Arabian Shield (Harris, 1985), Himalayan belt (Turner et al., 1996; Miller et al., 1999; Williams et al., 2004), Sulu belt (Yang et al., 2005a,b) and other examples (Sylvester, 1989; Guo et al., 2005). In addition, alkaline rocks (e.g., monzonites, syenites, A-type granites) are commonly intimately associated with alkaline mafic rocks (e.g., mafic dikes), especially alkali to transitional basalts (Yang et al., 2005a,b). As such, it is important to undertake detailed investigations of alkaline rocks, especially those alkaline associations within the Sulu high pressure (HP) to ultra-high pressure (UHP) metamorphic belt.

* Corresponding author. State Key Laboratory of Ore Deposit Geochemistry, Institute of Geochemistry, Chinese Academy of Sciences, Guiyang 550002, China. Tel.: +86 851 5895187; fax: +86 851 5891664.
E-mail address: liushen@vip.gyig.ac.cn (S. Liu).

0024-4937/$ – see front matter © 2008 Elsevier B.V. All rights reserved.
doi:10.1016/j.lithos.2008.09.004

At present, however, only one alkaline association—the Jiazishan Complex, exposed in the Sulu orogenic belt, has been reported upon (Lin et al., 1992; Chen et al., 2003; Yang et al., 2005a,b). Moreover, the origin of these rocks remains controversial (Yang et al., 2005a,b; Xie et al., 2006). Therefore, our work on the ~120 Ma alkaline intrusions and associated mafic dikes may provide further constraints on this debate and determine the petrogenetic processes occurring during a later evolutionary stage. In this paper we present SHRIMP U–Pb ages, major and trace element geochemistry and Sr–Nd–Pb–Hf isotope data for the juvenile alkaline associations of quartz–monzonite–A-type granite and mafic dikes from the central Sulu orogenic belt (Fig. 1). These data are used to discuss their petrogenesis and tectonic implications.

2. Geological setting and petrography

The Sulu terrane was offset by the sinistral Tanlu fault with a northerly displacement of about 500 km (Xu and Zhu, 1994). Along the ENE-trending Wulian–Qingdao–Rongcheng fault, the terrane is generally divided into two metamorphic terranes, i.e. a high-pressure blueschist unit to the south and an UHP metamorphic granitic gneiss, granulite and subordinate eclogite, schist, amphibolite, marble and quartzite association unit to the north (Cao et al., 1990; Zhai et al., 2000; Chen et al., 2003; Guo et al., 2004). The northern terrane also includes the Laiyang basin of Mesozoic age. Mesozoic magmatic rocks are widely distributed in the Sulu orogenic belt, and they mainly formed between 225 Ma and 114 Ma (Zhao et al., 1997; Zhou and Lu, 2000; Fan et al., 2001; Chen et al., 2003; Zhou et al., 2003; Guo et al., 2004, 2005; Huang et al., 2005; Meng et al., 2005; Yang et al., 2005a,b; Guo et al., 2006). The distribution of these Mesozoic mafic rocks is limited, and most of them are distributed as dikes (BGMRS, 1991b; Cheng et al., 1998; Yang and Zhou, 2001; Guo et al., 2004), only small-scale basalts and mafic intrusions are reported (Fan et al., 2001; Meng et al., 2005).

The studied area is located in the central section of the Sulu terrane from Junan to Jiaonan (Fig. 1). The alkaline association of quartz–monzonites, A-type granites and mafic dikes are investigated: the quartz–monzonites (JN1,7,9,14) and alkaline mafic dikes–dolerites (JNM2, 3, 8, 9,11,15) from Junan, the quartz–monzonites (DC1–3, 5, 6; DC2–2, 7, 9) from Dadian, the A-type granites (JX1, 7, 10) and alkaline dolerites (JXM3, 4, 7, 10, 11, 13) from Juxian, the A-type granites (WL2, 7, 12) from Wulian, and the quartz–monzonites (JC9, 12, 13) from Jiaonan (Fig. 1). Cross-cutting relationships indicate that the mafic dikes have been intruded after the felsic rocks. We describe each suite in turn.

2.1. Junan quartz–monzonites

The Junan quartz monzonitic intrusion is exposed for ca. 120 km^2; it intruded into Archean or lower Proterozoic gneisses (Fig. 1).

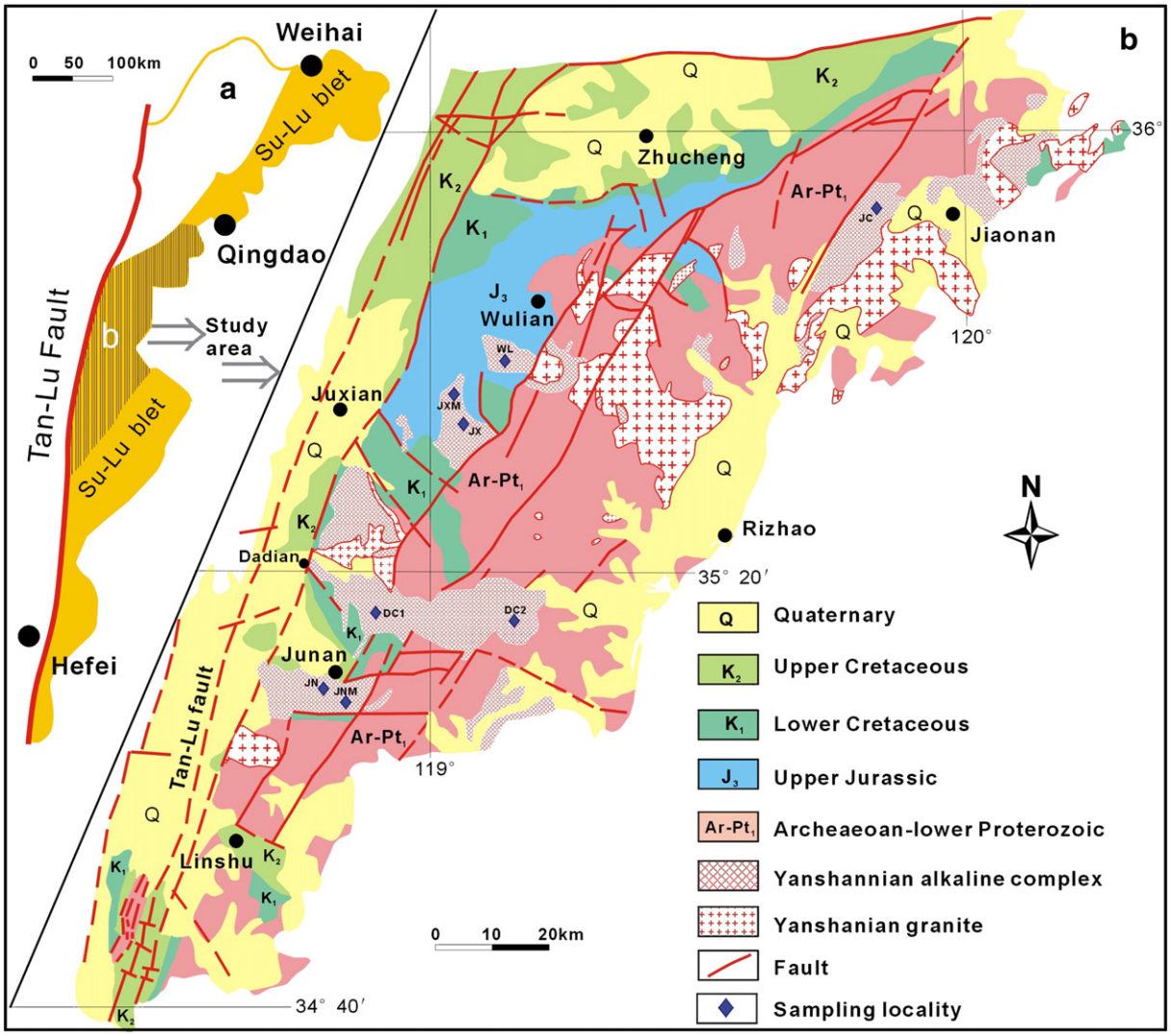

Fig. 1. a. Simplified tectonic map of the Sulu belt, eastern China (modified after Guo et al., 2004). b. The geologic map of study areas and the distributions of the alkaline intrusions and mafic dikes (modified after BGMRS, 1991a).

The monzonites are light grey, medium- to coarse-grained with granular and porphyritic textures. They are composed of subhedral orthoclase (38–40%) and quartz (10–13%), euhedral andesine (30–35%), and diopside (8–10%) with minor (3%) biotite and amphibole. Accessory minerals include apatite, zircon, magnetite and titanite.

2.2. Dadian quartz–monzonites

Dadian monzonite outcrops over ca. 550 km^2, and is the largest intrusion in the study area. It also intruded into the Archean or lower Proterozoic gneisses and was intruded by the Yanshanian granite (Fig. 1). The rocks are commonly light grey, medium- to coarse-grained with granular and porphyritic textures. The Dadian monzonite consists predominantly of K-feldspar (40–42%), quartz (10–15%), andesine (32–35%), diopside (8–10%), subordinate (2%) amphibole and biotite, and accessory minerals including apatite, zircon, magnetite and titanite.

2.3. Juxian A-type granites

The Juxian granite outcrops over 75 km^2; it intruded into upper Jurassic strata (Fig. 1). It is commonly light grey to pink in color, and composed of quartz (25–35%), perthite (25–45%), albite (An0–5) (15–18%), and minor muscovite. Accessory minerals include zircon, magnetite and apatite.

Table 1
Major oxides (wt.%) and trace elements for the representative felsic and mafic dikes in Sulu belt

Sample no.	JN1	JX1	DC1-3	DC2-2	WL2	JC9	JXM3	JXM4	JNM2	JNM3	GSR-3	GSR-3	GSR-1	GSR-1
Rock type	Quartz monzonite	Granite	Quartz monzonite	Quartz monzonite	Granite	Quartz monzonite	Dolerite	Dolerite	Dolerite	Dolerite	RV*	MV*	RV*	MV*
SiO_2	62.64	73.01	60.77	62.13	72.68	61.96	50.72	51.49	51.65	51.5	44.64	44.75	72.83	72.65
TiO_2	0.69	0.25	0.75	0.60	0.235	0.67	0.799	0.969	1.105	1.13	2.37	2.36	0.29	0.29
Al_2O_3	16.23	14.45	16.31	16.11	14.52	15.55	14.69	16.34	15.6	15.96	13.83	14.14	13.40	13.52
Fe_2O_3	5.52	1.92	5.81	5.41	1.91	5.2	8.35	7.39	8.96	8.71	13.4	13.35	2.14	2.18
MnO	0.10	0.07	0.11	0.11	0.07	0.10	0.12	0.14	0.16	0.18	0.17	0.16	0.06	0.06
MgO	2.33	0.42	2.47	2.35	0.39	2.38	9.86	5.59	6.62	6.11	7.77	7.74	0.42	0.46
CaO	3.94	1.28	4.11	3.73	1.26	3.91	7.74	7.59	7.67	7.44	8.81	8.82	1.55	1.56
Na_2O	3.46	3.84	3.69	3.95	3.95	4.41	2.50	3.00	2.80	3.03	3.38	3.18	3.13	3.15
K_2O	5.28	5.45	5.37	5.53	5.51	5.67	2.286	3.175	2.627	3.14	2.32	2.3	5.01	5.03
P_2O_5	0.35	0.08	0.38	0.44	0.07	0.43	0.42	0.91	0.46	0.47	0.95	0.97	0.09	0.11
LOI	0.12	0.01	0.34	0.04	0.12	0.04	2.32	2.93	1.94	2.11	2.24	2.12	0.70	0.69
Total	100.66	100.78	100.11	100.39	100.721	100.325	99.802	99.530	99.601	99.777	99.88	99.89	99.62	99.7
$Mg^{\#}$	45.5	30.2	45.7	46.2	28.8	47.5	70.0	60.0	59.4	58.1	OU-6 (RV*)	OU-6 (MV*)	GBPG-1 (RV*)	GBPG-1 (MV*)
V	83.5	15.9	107	99.5	17.0	99.3	162.3	153.9	17.9	188.9	129	131	96.5	103
Cr	35.4	7.92	35.6	58.6	11.9	27.5	577.8	64.5	9.3	224.5	70.8	73.5	181	187
Co	12.5	2.21	14.6	14.3	2.5	14.0	40.8	23.5	2.4	34.0	29.1	30.3	19.5	20.2
Ni	13.6	3.80	16.5	20.6	30.0	88.8	146.1	49.6	5.0	79.6	39.8	42.5	59.6	60.6
Cu	22.2	5.82	55.6	9.22	7.4	26.6	19.6	35.1	4.1	14.1	39.6	41.8	30.0	33.6
Zn	79.8	33.2	95.1	89.7	70.0	63.4	98.4	129.6	40.4	208.7	111	113	80.3	86.1
Ga	26.5	25.3	28.2	27.1	23.7	24.1	20.5	22.5	21.1	21.8	24.3	26.5	18.6	20.9
Rb	168	115	188	132	136	140	36.4	70.5	146	140	120	122	56.2	61.4
Sr	317	208	327	416	235	369	1171	1670	1234	1124	131	136	364	377
Y	21.5	18.0	26.0	21.5	19.5	22.8	19.3	23.2	19.5	25.2	27.4	26.2	18.0	17.2
Zr	265	291	287	277	334	368	181	249	103	261	174	183	232	224
Nb	18.4	16.8	19.0	15.9	17.1	19.1	6.7	9.9	17.1	8.9	14.8	15.3	9.93	8.74
Cs	1.95	1.20	3.57	1.56	1.1	2.4	0.3	2.2	1.2	3.1	8.02	8.30	0.32	0.34
Ba	1398	907	1237	1449	1036	1569	3860	7634	2872	3342	477	486	908	921
La	85.6	64.1	127	100	74.1	106.5	62.0	94.5	68.6	61.2	33.0	33	53.0	51
Ce	168	108	237	183	125	207	119	193	132	123.6	74.4	78	103	105
Pr	17.0	11.1	23.4	18.7	12.2	20.9	13.2	20.4	14.2	14.1	7.80	8.1	11.5	11.6
Nd	57.5	35.9	78.9	65.3	39.7	73.0	48.9	77.2	43.4	55.6	29.0	30.6	43.3	42.4
Sm	8.57	5.44	11.4	9.87	5.92	11.0	7.68	12.6	5.77	9.41	5.92	5.99	6.79	6.63
Eu	1.65	0.79	2.18	2.10	0.87	2.26	1.75	2.80	1.48	2.51	1.36	1.35	1.79	1.69
Gd	6.40	4.10	8.18	6.96	4.33	7.75	5.05	6.73	3.92	6.12	5.27	5.50	4.74	4.47
Tb	0.79	0.60	1.00	0.87	0.65	0.94	0.72	1.03	0.65	0.97	0.85	0.83	0.60	0.59
Dy	4.09	3.41	5.18	4.37	3.65	4.93	3.75	4.91	3.57	5.21	4.99	5.06	3.26	3.17
Ho	0.75	0.67	0.96	0.79	0.70	0.85	0.70	0.85	0.68	0.96	1.01	1.02	0.69	0.66
Er	2.29	2.01	2.76	2.23	2.14	2.49	2.03	2.36	2.14	2.71	2.98	3.07	2.01	2.02
Tm	0.32	0.30	0.39	0.30	0.31	0.34	0.26	0.30	0.29	0.36	0.44	0.45	0.30	0.29
Yb	2.20	1.97	2.57	1.97	2.19	2.32	1.74	1.87	2.12	2.24	3.00	3.09	2.03	2.03
Lu	0.34	0.30	0.38	0.29	0.34	0.33	0.26	0.28	0.32	0.34	0.45	0.47	0.31	0.31
Hf	5.78	6.35	8.02	6.16	10.38	11.0	4.02	5.01	3.31	5.47	4.70	4.86	6.07	5.93
Ta	0.91	0.83	0.37	0.33	0.39	0.48	0.10	0.14	0.96	0.70	1.06	1.02	0.40	0.46
Pb	27.5	26.5	28.7	24.6	25.2	24.5	13.5	24.4	20.2	21.5	28.2	32.7	14.1	14.5
Th	67.8	44.3	53.8	35.4	29.2	41.9	9.6	14.3	5.5	5.9	11.5	13.9	11.2	11.4
U	11.8	3.36	14.85	3.48	5.1	7.4	1.9	2.8	1.1	1.2	1.96	2.19	0.90	0.99
δEu	0.7	0.5	0.7	0.8	0.5	0.8	0.9	0.9	1.0	1.0				
T_{Zr}(°C)	856	889	858	856	903	874	–	–	–	–				

LOI = loss on ignition. $Mg^{\#} = 100*Mg/(Mg+\sum Fe)$ atomic ratio."–": not calculated. Note that T_{Zr} (°C) is calculated from zircon saturation thermometry (Watson and Harrison, 1983). RV*: recommended values; MV*: measured values; the values for GSR-1 and GSR-3 from Wang et al. (2003). The values for GBPG-1 from Thompson et al. (2000), and for OU-6 from Potts and Kane (2005).

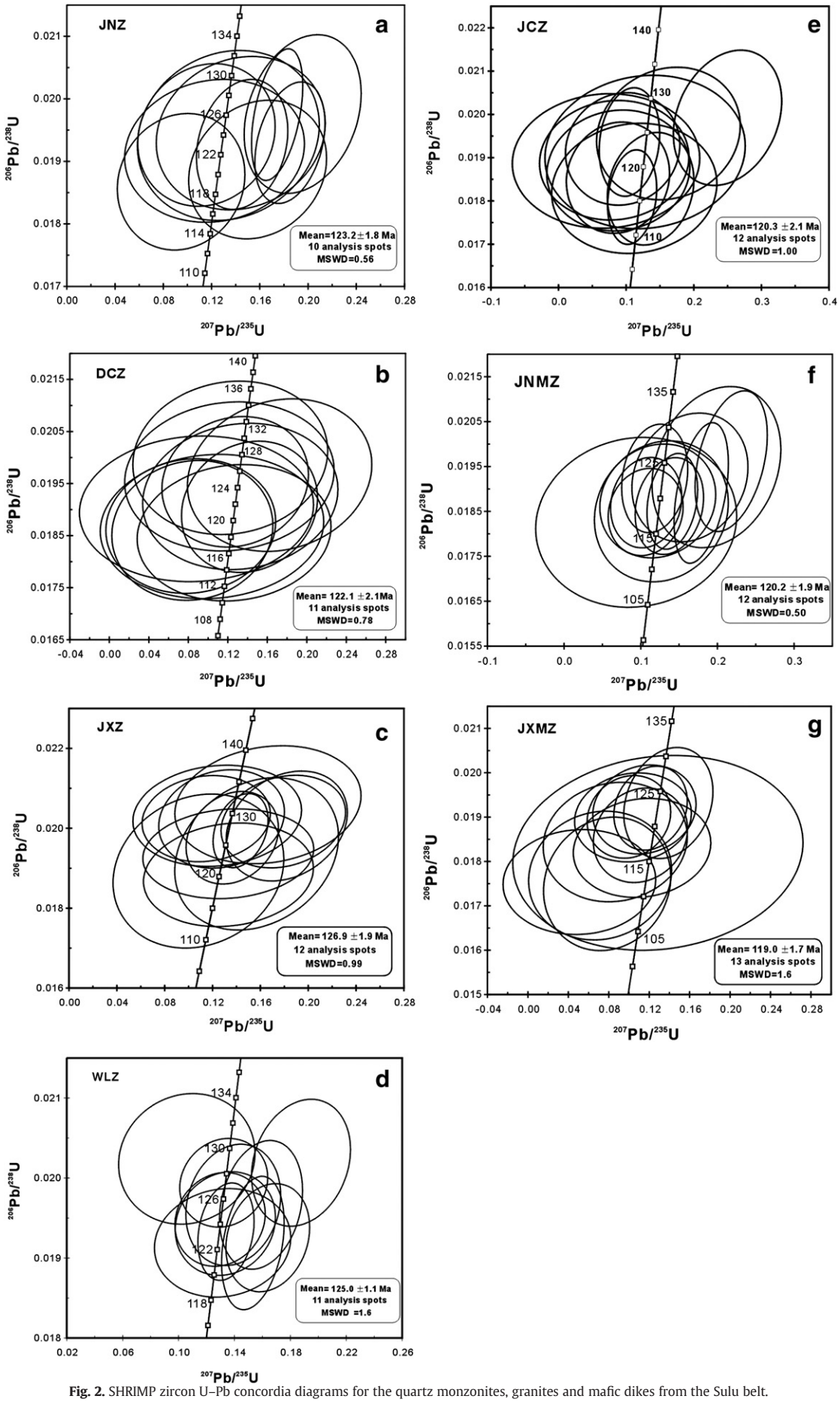

Fig. 2. SHRIMP zircon U–Pb concordia diagrams for the quartz monzonites, granites and mafic dikes from the Sulu belt.

2.4. Wuilan A-type granites

The Wulian granite (~90 km^2) also intruded into upper Jurassic strata (Fig. 1). The rocks are similar to Juxian granites in terms of color and composition.

2.5. Jiaonan Quartz–monzonites

The Jiaonan quartz monzonitic intrusion (~270 km^2) mainly intruded into Archean or lower Proterozoic gneisses. It is associated with the Yanshanian granites (Fig. 1). The rocks are light grey and characteristically medium- to coarse-grained with granular and porphyritic textures. They are dominated by K-feldspar (40–45%), quartz (10–15%), andesine (30–35%), minor amphibole and biotite (2–3%). Accessory minerals include apatite, zircon, magnetite and titanite.

2.6. Junan and Juxian mafic dikes

Mafic dikes intruded into Junan quartz–monzonites and Juxian A-type granites, respectively. The individual mafic dikes are vertical, and NE–SW-trending approximately 10–80 m wide and 4–5 km in length. The dikes are characterized by ~30–35% of micro- (0.5–1.2 mm) phenocrysts of clinopyroxene, alkali feldspar, plagioclase and minor biotite and ~65–70% of groundmass pyroxene, alkali feldspar, plagioclase, magnetite and chlorite. The dykes display doleritic textures.

3. Analytical procedures

3.1. SHRIMP zircon U–Pb method

Zircon was separated from three quartz monzonites and two granites (~4 kg) (JNZ, DCZ, JXZ, WLZ and JCZ), and two mafic dikes (JNMZ and JXMZ) (>30 kg) using conventional heavy liquid and magnetic techniques. Representative zircon grains were hand-picked under binocular microscope and mounted in an epoxy resin disc, and then polished and coated with a gold film. Zircons were documented with transmitted and reflected light as well as cathodoluminescence (CL) to reveal their external and internal structures. The U–Pb isotopic analyses were performed using the Sensitive High-Resolution Ion Microprobe (SHRIMP-II) at the Chinese Academy of Geological Sciences (Beijing) (Table 1 in the Appendix). Procedures are described in detail by Compston et al. (1992), Williams (1998) and Song et al. (2002). The U–Pb isotope data were collected after five scans and a reference zircon TEM (417 Ma) (Black et al., 2003) was analyzed after every four spots. The uncertainties in ages are cited as 1σ, and the weighted mean ages are quoted at the 95% confidence level (2σ).

3.2. Major, trace elemental and isotopic analyses

Thirty-one samples were collected to carry out major and trace element determinations and Sr–Nd–Pb isotopic analyses. Whole-rock samples were trimmed to remove altered surfaces, and were cleaned with deionized water, crushed and powdered with an agate mill.

Major elements were analyzed with a PANalytical Axios—advance (Axios PW4400) X-ray fluorescence spectrometer (XRF) at the State Key Laboratory of Ore Deposit Geochemistry, Institute of Geochemistry, Chinese Academy of Sciences (IGCAS). Fused glass disks were used and the analytical precision as determined on the Chinese National standard GSR-1 and GSR-3 was better than 5% (Table 2 in the Appendix). Loss on ignition (LOI) was obtained using 1 g powder heated up to 1100 °C for 1 h.

Trace elements were analyzed with a POEMS ICP-MS at the National Research Center of Geoanalysis, Chinese Academy of Geosciences, following procedures described by Qi et al. (2000). The discrepancy between the triplicates is less than 5% for all the elements. Analyses of international standards OU-6 and GBPG-1 are in agreement with the recommended values (Table 1).

For Rb–Sr and Sm–Nd isotope analyses, sample powders were spiked with mixed isotope tracers, dissolved in Teflon capsules with HF+ HNO_3 acids, and separated by conventional cation-exchange technique. Isotopic measurements were performed on a Finnigan MAT-262 thermal ionization mass spectrometer (TIMS) at the Isotopic Geochemistry Laboratory of Yichang Institute of Geology and Minerals resources. Procedural blanks were <200 pg for Sm and Nd and <500 pg for Rb and Sr. The mass fractionation corrections for Sr and Nd isotopic ratios were based on $^{86}Sr/^{88}Sr=0.1194$ and $^{146}Nd/$

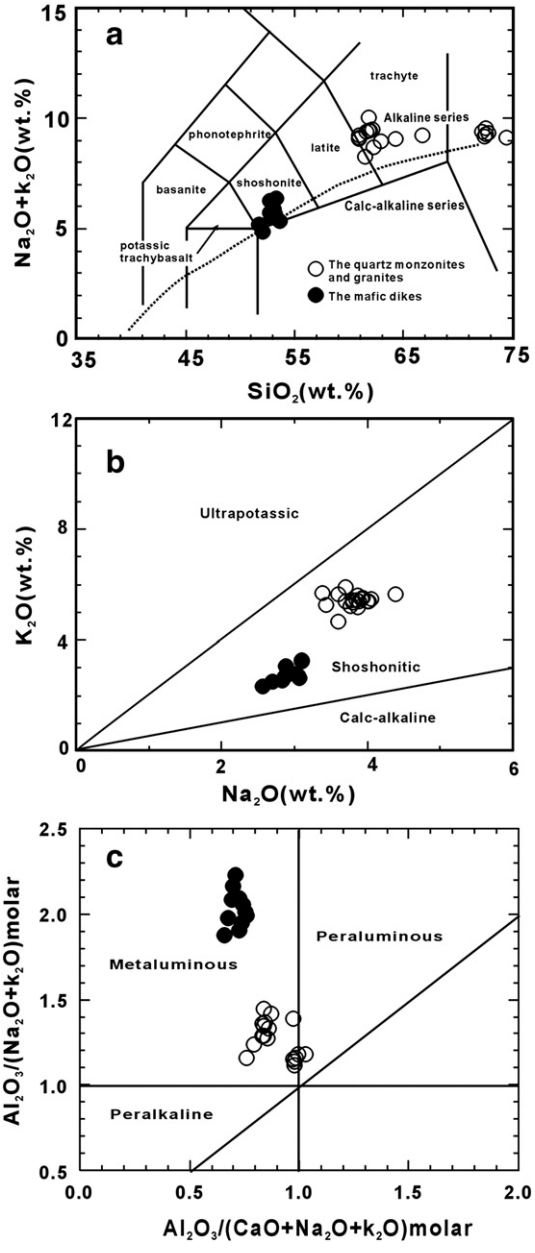

Fig. 3. Classification of the monzonites, granites and mafic dikes from the Sulu belt on the basis of (a) the TAS diagram. All the major element data have been recalculated to 100% on a LOI-free basis (after Middlemost, 1994; Le Maitre, 2002); (b) K_2O vs. Na_2O diagram, showing the alkaline association to be shoshonitic (after Middlemost, 1972); (c) $Al_2O_3/(Na_2O+K_2O)$ molar vs. $Al_2O_3/(CaO+Na_2O+K_2O)$ molar plot. Most samples fall in the metaluminous field except some samples straddle the metaluminous and peralkaline boundary. Legends in other figures are the same as in this figure.

$^{144}Nd = 0.7219$, respectively. Analyses of standards during the period of analysis are as follows: NBS987 gave $^{87}Sr/^{86}Sr = 0.710246 \pm 16 (2\sigma)$; La Jolla gave $^{143}Nd/^{144}Nd = 0.511863 \pm 8$ (2σ). Pb was separated and purified by conventional cation-exchange technique (AG1×8, 200–400 resin) with diluted HBr as eluant. Analyses of NBS981 during the period of analysis yielded $^{204}Pb/^{206}Pb = 0.0896 \pm 15$, $^{207}Pb/^{206}Pb = 0.9145 \pm 8$, and $^{208}Pb/^{206}Pb = 2.162 \pm 2$.

3.3. In situ zircon Hf isotopic analysis

In situ zircon Hf isotopic analyses were conducted using a Neptune MC-ICPMS, equipped with a 193 nm laser, at the Institute of Geology and Geophysics, Chinese Academy of Sciences in Beijing, China. During analysis, a laser repetition rate of 10 Hz at 100 mJ was used and spot sizes of 32 and 63 μm. Raw count rates for ^{172}Yb, ^{173}Yb, ^{175}Lu, $^{176}(Hf+Yb+Lu)$, ^{177}Hf, ^{178}Hf, ^{179}Hf, ^{180}Hf and ^{182}W were collected and isobaric interference corrections for ^{176}Lu and ^{176}Yb on ^{176}Hf must be determined precisely.^{176}Lu was calibrated using the ^{175}Lu value and the correction was made to ^{176}Hf. The $^{176}Yb/^{172}Yb$ value of 0.5887 and mean β_{Yb} value obtained during Hf analysis on the same spot were applied for the interference correction of ^{176}Yb on ^{176}Hf (Iizuka and Hirata, 2005). The detailed analytical technique is described in Xu et al. (2004) and Wu et al. (2006). During analysis, the $^{176}Hf/^{177}Hf$ and $^{176}Lu/^{177}Hf$ ratios of the standard zircon (91500) were 0.282300 ± 15 ($2\sigma_n$, n = 24) and 0.00030, similar to the commonly accepted $^{176}Hf/^{177}Hf$ ratio of 0.282302 ± 8 and $0.282306 \pm$

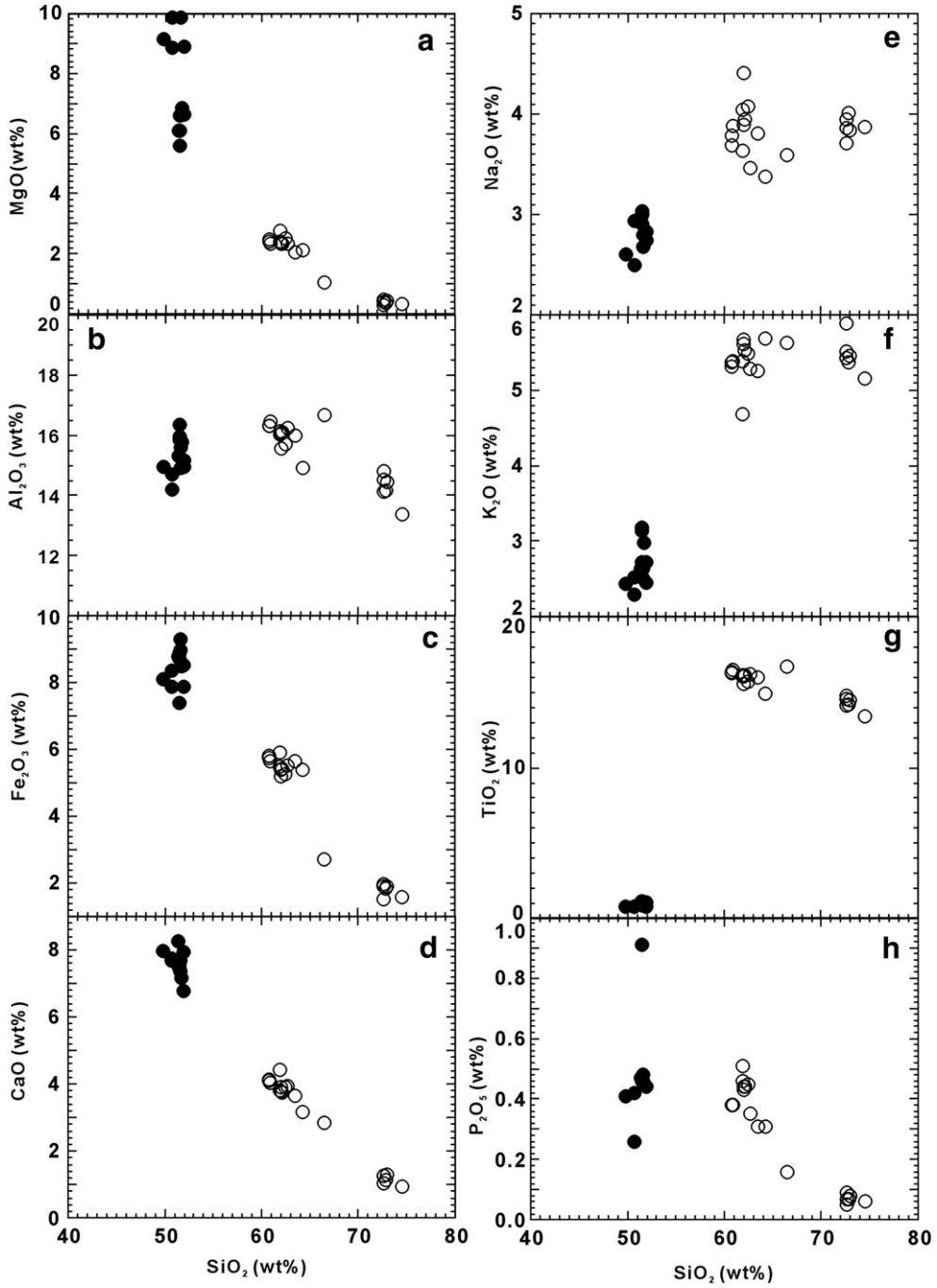

Fig. 4. Selected variation diagrams of major element oxides vs. MgO plots for the alkaline felsic rocks and mafic dikes from the Sulu belt.

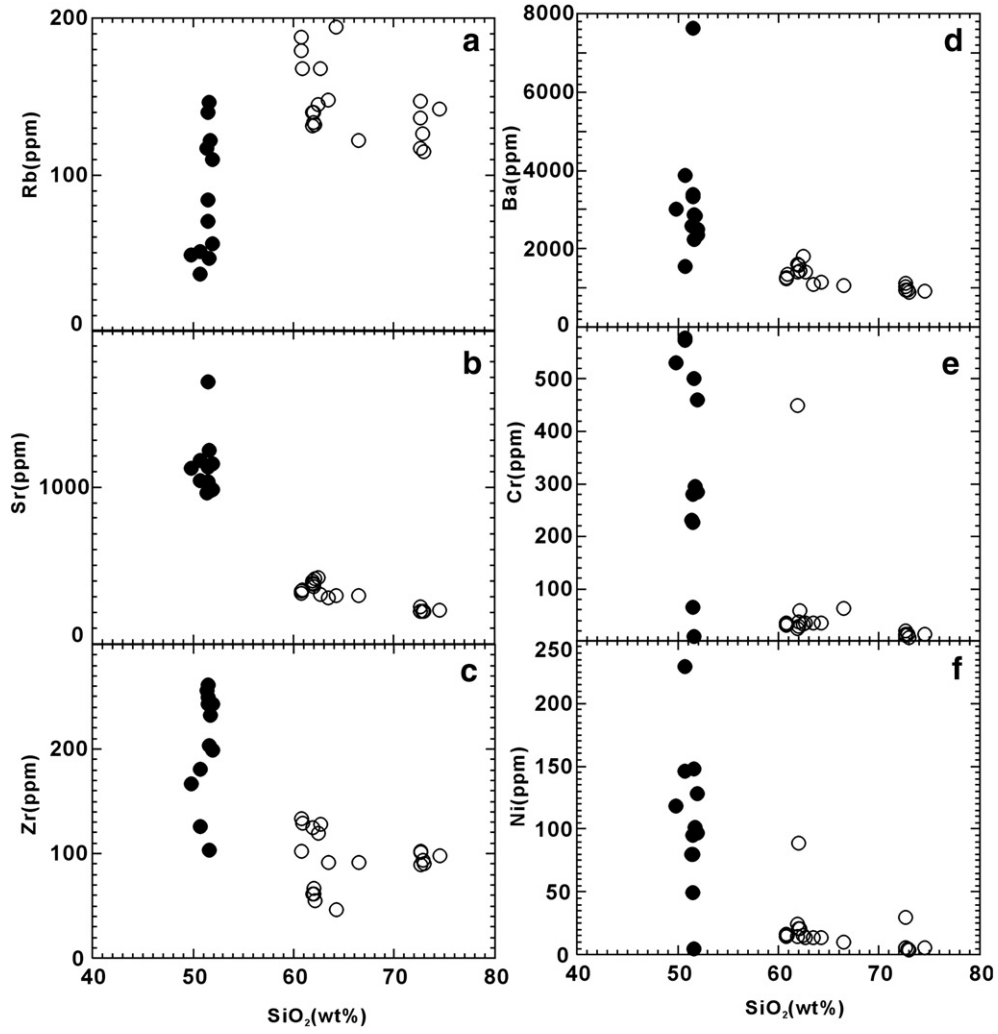

Fig. 5. Selected variation diagrams of trace elements vs. MgO plots for the alkaline felsic rocks and mafic dikes from the Sulu belt.

8 (2σ) measured using the solution method (Goolaerts et al., 2004; Woodhead et al., 2004).

4. Results

4.1. Zircon U–Pb ages

4.1.1. Sample JNZ from Junan quartz monzonite

Euhedral zircon grains in JNZ are clean and show prismatic form with magmatic oscillatory zoning. Apart from one analysis of a slightly older grain (spot 2.1) and one analysis of a highly juvenile grain (spot 12.1 with the age of 42.9 Ma), ten grains yielded a weighted mean $^{206}Pb/^{238}U$ age of 123.2 ± 1.8 Ma (2σ) (95% confidence interval) (Table 1 in the Appendix and Fig. 2a), which is the best estimate of the crystallization age for sample JNZ. The rejected analysis of spot 2.1 yields a $^{206}Pb/^{238}U$ age of 227 Ma, and is interpreted to be an inherited zircon age.

4.1.2. Sample DCZ from Dadian quartz monzonite

Zircons are mostly clear and euhedral with concentric zoning. Twelve analyses of 12 zircons were obtained (Table 1 in the Appendix), excluding one slightly younger grain (spot 5.1), eleven zircons yielded a weighted mean age of 122.1 ± 2.1 Ma (2σ) (Fig. 2b).

4.1.3. Sample JXZ from Juxian granite

Zircons are euhedral and most show concentric zoning; no inherited zircon core was observed. Twelve analyses of 12 zircons were obtained (Table 1 in the Appendix), and yielded a weighted mean $^{206}Pb/^{238}U$ age of 126.9 ± 1.9 Ma (Fig. 2c), which is the best estimate of the crystallization age of this sample.

4.1.4. Sample WLZ from Wulian granite

Zircons are mostly clear and euhedral with concentric zoning. Thirteen analyses of 13 zircons were obtained (Table 1 in the Appendix).

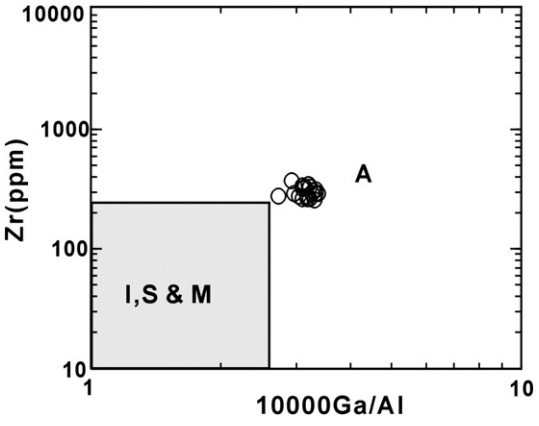

Fig. 6. Plots of the alkaline quartz monzonites and granites in Zr vs. 10,000×Ga/Al diagram of Whalen et al. (1987) showing affinity of A-type granites.

Apart from two analyses of slightly older grains (spots 6.1 and 13.1), eleven zircons yielded a weighted mean age of 125.0±1.1 Ma (Fig. 2d), which is the best estimate of the crystallization age of sample WLZ.

4.1.5. Sample JCZ from Jiaonan quartz monzonite

Zircons are mostly clear and euhedral with concentric zoning, thirteen analyses of 13 zircons were obtained (Table 1 in the Appendix), one spot was rejected with a very young age (spot 3.1 with an age of 18.2 Ma), the other twelve analyses of 12 zircons gave a weighted mean $^{206}Pb/^{238}U$ age of 120.3±2.1 Ma (95% confidence interval) (Fig. 2e), which is the best estimate of the crystallization age of sample JCZ.

4.1.6. Sample JNMZ from Junan mafic dike

Zircons are euhedral and most of them show magmatic concentric zoning; no inherited zircon was observed, and twelve analyses of 12 zircons were obtained (Table 1 in the Appendix). These yielded a weighted mean age of 120.2±1.9 Ma (95% confidence interval) (Fig. 2f), which is the best estimate of crystallization age of sample JNMZ.

4.1.7. Sample JXMZ from Juxian mafic dike

The majority of the zircon grains are euhedral with concentric zoning. Thirteen analyses of 13 zircons were obtained (Table 1 in the Appendix). Apart from one slightly younger analysis (spot 3.1), the other twelve analyses yielded a weighted mean $^{206}Pb/^{238}U$ age of 119.0±1.7 Ma (Fig. 2g), which is the best estimate of the crystallization age of sample JXMZ.

4.2. Major and trace elements

Geochemical data for the quartz monzonites, granite and mafic dikes from Sulu orogenic belt are listed in Table 1.

The quartz monzonites, granite and mafic dikes have a wide range of chemical compositions, with SiO_2=49.87–74.49 wt.%, Al_2O_3=13.3–16.67wt.%, MgO=0.31–9.86 wt.%, Fe_2O_3=1.52–9.29 wt.%, CaO=0.95–8.25 wt.%. They are relatively high in total alkalis, with K_2O=2.29–5.89 wt.% and Na_2O=2.50–4.41 wt.%, and the total K_2O+Na_2O ranging from 4.78 wt.% to 10.08 wt.%. All felsic rocks and a majority of the mafic dikes plot in the alkaline field on the total alkali-silica (TAS) diagram (Fig. 3a). In addition, all samples straddle the shoshonitic series in the Na_2O vs. K_2O plot (Fig. 3b). In a plot of molar ratios of $Al_2O_3/(Na_2O+K_2O)$ and $Al_2O_3/(CaO+Na_2O+K_2O)$, the rocks are mostly metaluminous except some samples falling along the boundary of metaluminous and peralkaline (Fig. 3c). The quartz monzonites and granites display regular trends of decreasing MgO, Al_2O_3, Fe_2O_3, CaO, TiO_2, P_2O_5, Zr, Sr and Ba with increasing SiO_2 (Figs. 4 and 5), and weak correlations between Na_2O, K_2O, Rb and SiO_2. Additionally, Ni and Cr remain nearly constant with the exception of one sample (Fig. 5). In contrast, there are no correlations between SiO_2 and other elements for the mafic dikes (Figs. 4 and 5). The 10,000×Ga/Al ratios of the monzonites and granites range from 2.73 to 3.37. In the Ga/Al vs. Zr discrimination diagram (Fig. 6) of Whalen et al. (1987), the felsic rocks are all classified as A-type granite.

The quartz monzonites and granites are all characterized by LREE enrichment and HREE depletion, with a wide range La_N/Yb_N values (18–38) and moderate or small negative Eu anomalies (Eu/Eu*=0.5–0.8) (Fig. 7a). The chondrite-normalized REE patterns of the mafic dikes (Fig. 7b) are analogous to those of felsic rocks, showing relative enrichment of LREE over HREE (La_N/Yb_N=18–34) but without negative Eu anomalies. On average, the total REE contents of the mafic dikes are lower than those of the quartz monzonites, but higher than those of the granites. In the primitive mantle-normalized trace element diagrams, quartz monzonites and granites show enrichment in LILEs (i.e., Rb, Pb, Th and U) and depletion in Ba, Sr and HFSEs (i.e., Nb, Ta and Ti) (Fig. 7c). The

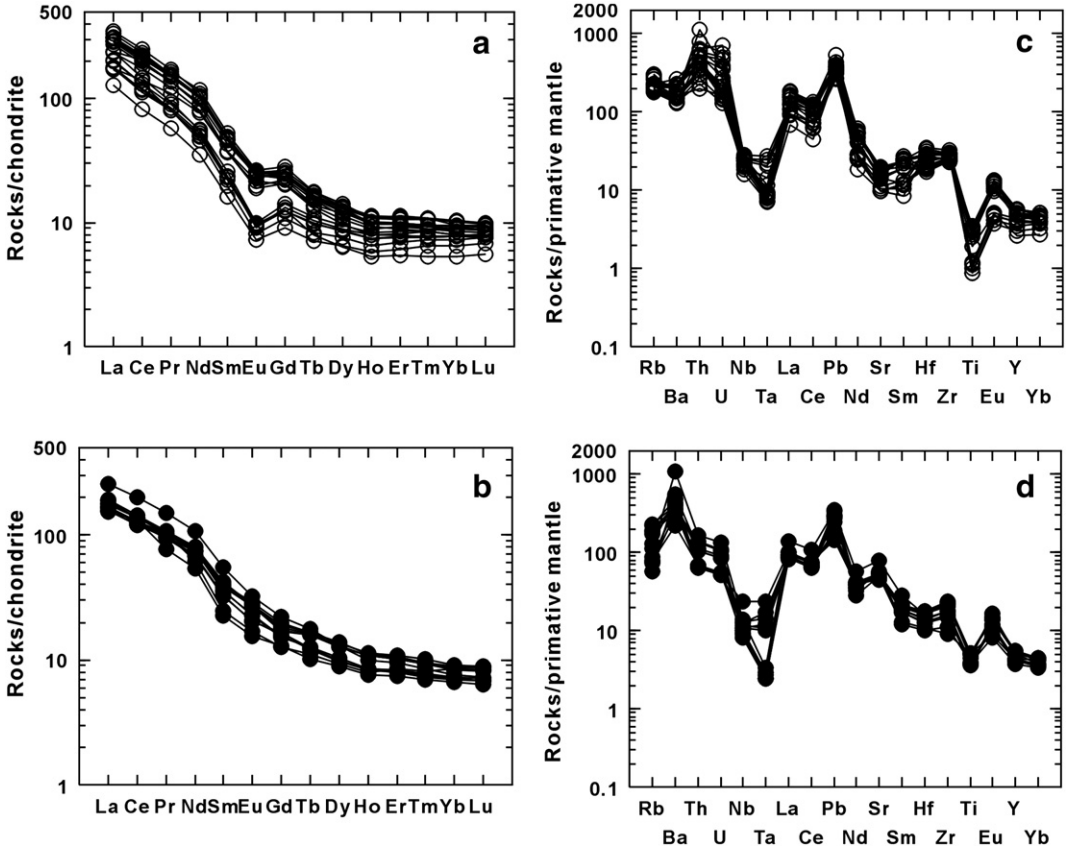

Fig. 7. Chondrite-normalized REE diagrams and primitive mantle-normalized incompatible element distribution spidergrams for the (a, c) quartz monzonites and granites and (b, d) mafic dikes from the Sulu belt. The normalization values are from Sun and McDonough (1989).

Table 2
Sr–Nd–Pb isotopic compositions for the alkaline felsic rocks and mafic dikes in Sulu belt

Sample no.	Age(Ma)	Sm (ppm)	Nd (ppm)	$^{147}Sm/^{144}Nd$	$^{143}Nd/^{144}Nd$	2σ	$(^{143}Nd/^{144}Nd)_i$	$\varepsilon_{Nd}(t)$	Rb (ppm)	Sr (ppm)	$^{87}Rb/^{86}Sr$	$^{87}Sr/^{86}Sr$	2σ	$(^{87}Sr/^{86}Sr)_i$	$^{206}Pb/^{204}Pb$	$^{207}Pb/^{204}Pb$	$^{208}Pb/^{204}Pb$
JN1		9.72	66.74	0.088	0.511685	9	0.511614	−16.9	169	776	0.541	0.709312	12	0.7084	17.092	15.424	37.701
JN7	123.2	8.67	54.50	0.096	0.511702	8	0.511624	−16.7	147	666	0.548	0.709728	11	0.7088	17.142	15.515	38.061
JN9		15.32	83.80	0.111	0.511682	11	0.511593	−17.3	192	659	0.723	0.709547	12	0.7083	17.149	15.511	38.043
JN14		5.45	38.01	0.087	0.511692	9	0.511622	−16.7	124	703	0.438	0.709451	10	0.7087	17.112	15.404	37.714
JX1		5.39	36.11	0.090	0.511584	10	0.511509	−18.8	115	208	1.370	0.710903	12	0.7084	16.442	15.412	37.177
JX7	126.9	5.53	38.49	0.087	0.511584	12	0.511512	−18.8	122	221	1.369	0.710825	10	0.7084	16.54	15.488	37.355
JX10		5.11	34.78	0.089	0.511595	14	0.511521	−18.6	128	208	1.523	0.711187	11	0.7084	16.874	15.618	38.248
DC1-3		11.38	78.96	0.087	0.511638	9	0.511569	−17.8	188	813	0.573	0.709142	9	0.7081	16.938	15.445	37.882
DC1-5	122.1	11.12	74.21	0.091	0.511647	8	0.511575	−17.7	178	851	0.520	0.709148	12	0.7082	16.966	15.47	37.933
DC1-6		10.73	73.54	0.088	0.511639	11	0.511569	−17.8	169	864	0.486	0.709011	16	0.7082	16.938	15.416	37.727
DC2-2		10.10	65.40	0.093	0.511695	10	0.511620	−16.8	133	1023	0.323	0.709443	14	0.7089	17.143	15.521	38.111
DC2-7	122.1	10.66	71.98	0.090	0.511694	12	0.511622	−16.7	133	1008	0.326	0.709144	13	0.7086	17.139	15.435	37.846
DC2-9		11.07	71.60	0.093	0.511696	8	0.511621	−16.8	131	1025	0.317	0.709402	10	0.7089	17.032	15.315	37.744
WL2		5.96	40.48	0.089	0.511578	11	0.511505	−19.0	135	234	1.431	0.711026	10	0.7085	16.754	15.535	37.477
WL7	125	3.41	23.54	0.087	0.511577	12	0.511505	−19.0	115	141	2.022	0.711943	11	0.7084	16.485	15.478	37.263
WL12		3.72	24.93	0.090	0.511578	11	0.511504	−19.0	147	206	1.770	0.711685	10	0.7085	16.417	15.452	37.146
JC9		10.41	71.93	0.087	0.511651	7	0.511582	−17.6	118	1146	0.256	0.708856	11	0.7084	16.882	15.382	37.544
JC12		10.68	70.26	0.092	0.511651	9	0.511579	−17.6	122	1163	0.261	0.708828	10	0.7084	16.913	15.408	37.634
JC13	120.3	11.31	73.95	0.092	0.511649	10	0.511576	−17.7	134	1064	0.312	0.709061	8	0.7085	16.982	15.41	37.759
JXM3		7.70	49.31	0.094	0.511572	10	0.511499	−19.2	37	1172	0.077	0.708841	11	0.7087	17.103	15.43	37.563
JXM4		12.57	77.48	0.098	0.511586	13	0.511910	−19.0	71	1672	0.105	0.708785	10	0.7086	17.198	15.634	38.034
JXM11	119	5.39	28.07	0.116	0.511650	11	0.511560	−18.1	51	637	0.200	0.708282	10	0.7079	17.246	15.607	38.449
JXM13		8.31	53.68	0.094	0.511702	11	0.511629	−16.7	47	1013	0.115	0.708918	13	0.7087	17.196	15.458	37.687
JNM2		5.76	42.96	0.081	0.511692	10	0.511628	−16.7	146	233	1.550	0.711253	8	0.7086	17.038	15.493	37.577
JNM3	120.2	9.38	55.36	0.102	0.511701	9	0.511620	−16.8	140	1124	0.308	0.708519	14	0.7080	16.97	15.432	37.435
JNM9		8.96	52.09	0.104	0.511692	12	0.511610	−17.0	111	986	0.279	0.708406	11	0.7079	16.987	15.458	37.538
JNM15		9.32	52.10	0.108	0.511785	9	0.511700	−15.3	84	1031	0.201	0.708442	13	0.7081	17.030	15.432	37.462

Chondrite Uniform Reservoir (CHUR) values ($^{87}Rb/^{86}Sr=0.0847$, $^{87}Sr/^{86}Sr=0.7045$, $^{147}Sm/^{144}Nd=0.1967$ $^{143}Nd/^{144}Nd=0.512638$) are used for the calculation. $\lambda_{Rb}=1.42\times10^{-11}$ year^{-1} (Steiger and Jäger, 1977); $\lambda_{Sm}=6.54\times10^{-12}$ year^{-1} (Lugmair and Harti, 1978).

mafic dikes have similar patterns but with positive Ba and Sr anomalies (Fig. 7d).

4.3. Sr, Nd and Pb isotopes

Sr, Nd and Pb isotopic data have been obtained from representative quartz monzonites, granites and mafic dikes samples (Table 2). The felsic and mafic rocks show very uniform $(^{87}Sr/^{86}Sr)_i$ ranging from 0.7079 to 0.7089 and relatively small variation in initial. $\varepsilon_{Nd}(t)$ values from −16.7 to −19.2 (with the exception of one relatively higher value, −15.3) , which suggests a common source region. In addition, the Sr–Nd isotopic compositions (Fig. 8) are comparable to those of the late Mesozoic volcanic rocks, alkaline complex, granites and mafic dikes, granites and diorites, gabbros, lamprophyres and adakites from the Sulu orogenic belt (Zhao et al., 1997; Zhou and Lu, 2000; Fan et al., 2001; Guo et al., 2004; Huang et al., 2005; Meng et al., 2005; Yang et al., 2005a,b; Guo et al., 2006) (Fig. 8).

The Pb isotopic ratios in felsic rocks and mafic dikes are characterized by $^{206}Pb/^{204}Pb=16.54–17.25$, $^{207}Pb/^{204}Pb=15.38–15.63$, $^{208}Pb/^{204}Pb=37.15–38.45$. They are significantly different from those of the Yangtze lithospheric mantle (Yan et al., 2003), and are identical to those of Jiazishan alkaline complex and mafic rocks from the central North China craton and Dabie orogen (Yan et al., 2003; Zhang et al., 2004; Xie et al., 2006), having a clear EM I affinity (Fig. 9a, b).

4.4. Zircon Hf isotopes

Zircon Hf isotope results are listed in Table 3 in the Appendix.

Fifteen spot analyses were obtained for sample JNZ, yielding very uniform $\varepsilon_{Hf}(t)$ values of between −21.4 and −22.9, corresponding to T_{DM2} model ages of between 2395 Ma and 2458 Ma, and giving an average of $\varepsilon_{Hf}(t)=-22.2\pm0.3$ and $T_{DM2}=2488\pm17$ Ma.

Nineteen spot analyses were obtained for sample DCZ; they show a narrow range of $\varepsilon_{Hf}(t)$ values between −21.1 and −22.5, corresponding to T_{DM2} model ages between 2364 Ma and 2465 Ma, and yielded a mean $\varepsilon_{Hf}(t)=-21.8\pm0.4$ and $T_{DM2}=2424\pm23$ Ma.

Nineteen spot analyses were made for sample JXZ. The determined $\varepsilon_{Hf}(t)$ values vary between −22.0 and −26.1, corresponding to T_{DM2} model ages in the range from 2433 Ma to 2684 Ma. These nineteen spots gave a mean $\varepsilon_{Hf}(t)=-23.7\pm1.0$ and $T_{DM2}=2540\pm62$ Ma.

Sixteen spot analyses were obtained for sample WLZ, giving $\varepsilon_{Hf}(t)$ values between −21.7 and −24.9, corresponding to T_{DM2} model ages between 2441 Ma and 2655 Ma, thus yielding an average of $\varepsilon_{Hf}(t)=-23.7\pm0.8$ and $T_{DM2}=2540\pm49$ Ma.

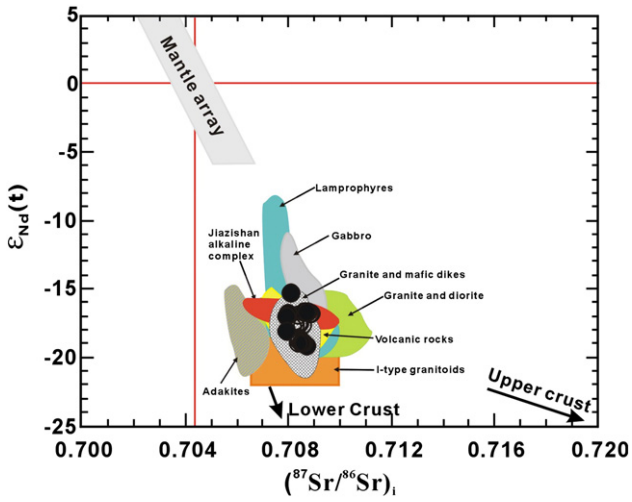

Fig. 8. Initial $^{87}Sr/^{86}Sr$ vs. $\varepsilon_{Nd}(t)$ diagram for the felsic rocks and mafic dikes from the Sulu belt. Other igneous rocks from the Sulu belt are also plotted: volcanic rocks from Fan et al. (2001) and Guo et al. (2004); Jiazishan alkaline complex is after Yang et al. (2005a); Granites and mafic dikes are after Yang et al. (2005b); Granite and diorite is after Huang et al. (2005); Gabbro is after Meng et al. (2005); Lamprophyres are after Guo et al. (2004); Adakites are from Guo et al. (2006); I-type granitoids are from Zhao et al. (1997) and Zhou and Lu (2000).

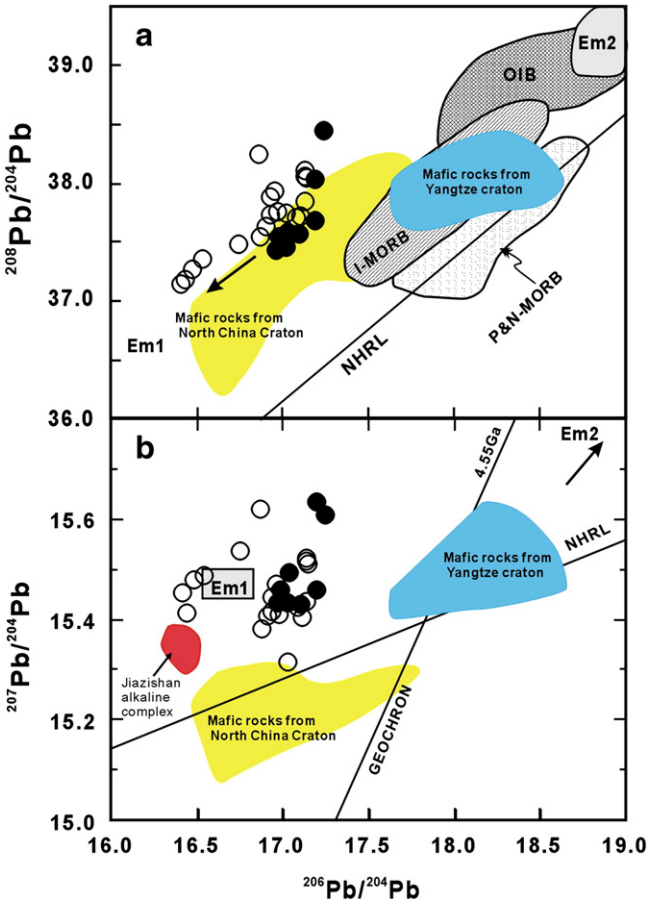

Fig. 9. $^{208}Pb/^{204}Pb$ and $^{207}Pb/^{204}Pb$ vs. $^{206}Pb/^{204}Pb$ diagrams for the alkaline felsic rocks and mafic dikes, compared with those of Early Cretaceous mafic rocks from the North China and Yangtze cratons. Fields for I-MORB (Indian MORB) and P&N-MORB (Pacific and North Atlantic MORB), OIB, NHRL and 4.55 Ga geochron are after Barry and Kent (1998), Zou et al. (2000), and Hart (1984), respectively. Data of North China craton are from Zhang et al., 2004 and Xie et al. (2006), Yangtze mafic rocks are after Yan et al. (2003).

Nineteen spot analyses were made for sample JCZ. The calculated $\varepsilon_{Hf}(t)$ values spread between −19.8 to −23.1, their T_{DM2} model ages range from 2302 Ma and 2501 Ma, corresponding to a mean $\varepsilon_{Hf}(t)$= −21.6±0.6 and T_{DM2}=2407±37 Ma.

Nineteen spot analyses were obtained for sample JNMZ, giving the $\varepsilon_{Hf}(t)$ values between −21.1 and −23.5, corresponding to T_{DM2} model ages between 2381 Ma and 2522 Ma. The nineteen analyses yielded a mean $\varepsilon_{Hf}(t)$=−22.4±0.5 and T_{DM2}=2458±29 Ma.

Nineteen spot analyses of sample JXMZ yielded $\varepsilon_{Hf}(t)$ values between −21.1 and −22.5, and T_{DM2} model ages between 2379 Ma and 2492 Ma, corresponding to a mean $\varepsilon_{Hf}(t)$=−22.0±0.4 and T_{DM2}=2436± 27 Ma.

Collectively, these results suggest that the felsic rocks and mafic dikes have close similarities in Hf isotopic compositions (average, $\varepsilon_{Hf}(t)$=−21.6 to −23.7), and indicate that parental magmas of the felsic rocks were derived from a similar source to the mafic dikes.

5. Discussion

5.1. Petrogenesis

5.1.1. Mantle source

The mafic dikes are characterized by low SiO_2 (49.87–51.92 wt.%), high MgO (5.59–9.86 wt.%), as well as elevated $Mg^{\#}$ (58–70), suggesting that they were derived from a mantle source rather than crust, as partial melting of any of the crustal rocks (e.g., Hirajima et al., 1990; Yang et al., 1993; Zhang et al., 1994, 1995; Kato et al., 1997) and lower crustal intermediate granulites (Gao et al., 1998a,b) in the deep crust would produce high-Si, low-Mg liquids (i.e., granitoid liquids; Rapp et al., 2003). The high initial $^{87}Sr/^{86}Sr$ ratios and negative $\varepsilon_{Nd}(t)$ and zircons $\varepsilon_{Hf}(t)$ values (Table 2 and Table 3 in the Appendix) for the mafic dikes are consistent with derivation from an enriched lithospheric mantle source.

The quartz monzonites and granitoids have Sr–Nd isotopic signatures largely overlapping with the associated mafic dikes and contemporaneous Rushan gabbros (<120 Ma) (Meng et al., 2005) and the other mafic intrusive and extrusive rocks (Fan et al., 2001; Guo et al., 2004; Yang et al., 2005b) in the Sulu belt (Fig. 8), favoring their derivation from basaltic magmas similar to the parental magmas of the mafic dikes. This is further supported by the very uniform zircons Hf isotopic compositions of these rocks.

5.1.2. Crustal assimilation

Assimilation, crystal fractionation (AFC) or magma mixing are usually postulated to explain the occurrence of comagmatic mafic and felsic rocks (e.g., DePaolo, 1981; Devey and Cox, 1987; Marsh, 1989; Mingram et al., 2000). AFC process and magma mixing would result in positive correlation between MgO and $\varepsilon_{Nd}(t)$ values, and negative correlation between MgO and $(^{87}Sr/^{86}Sr)_i$ ratios (Fig. 10). These features, however, are not observed either in the studied felsic rocks or mafic dikes, indicating that magma evolution is not significantly affected by crustal contamination or magma mixing. It is concluded that the geochemical and Sr–Nd–Hf isotopic signatures of the felsic rocks and mafic dikes were mainly inherited from an enriched mantle source.

5.1.3. Fractional crystallization

The positive correlations between MgO and Fe_2O_3, CaO, Cr and Ni in the mafic dikes (not presented) indicate that the mafic dikes were the result of olivine and pyroxene-dominated fractionation of a mafic magma. Moreover, the negative correlations between MgO and Al_2O_3 demonstrate that plagioclase was not a major fractionating phase for

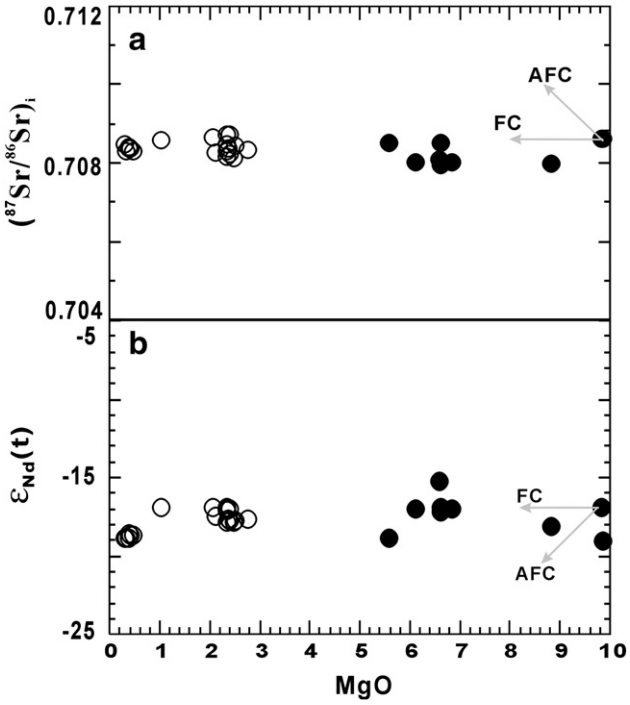

Fig. 10. Plots of (a) initial $^{87}Sr/^{86}Sr$ ratio and (b) $\varepsilon_{Nd}(t)$ value vs. MgO for the alkaline rocks from the Sulu belt, indicating crystal fractionation. FC: fractional crystallization; AFC: assimilation and fractional crystallization.

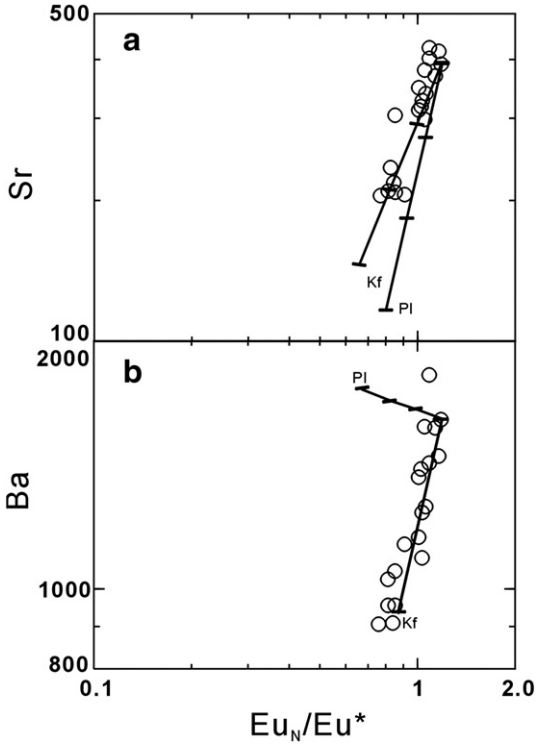

Fig. 11. Plots of (a) Eu_N/Eu^* vs. Sr, and (b) Ba vs. Sr for the quartz monzonites and granites. Mineral fractionation vectors calculated using partition coefficients from Philpotts and Schnetzler (1970), Schnetzler and Philpotts (1970) and Bacon and Druitt (1988). Tick marks indicate percentage of mineral phase removed, in 10% intervals. pl—plagioclase; kf—potassium keldspar.

the mafic dikes, which is further supported by the absence of negative Sr and Eu anomalies (Fig. 7b). Nevertheless, the high $Mg^{\#}$ (58–70) of the mafic dikes is inconsistent with significant fractionation. Comparatively, the monzonites and granites have relatively negative Ba, Sr and Eu anomalies (Fig. 7a and c), implying fractionation of potassium feldspar and plagioclase. The calculated effects of fractional crystallization are shown in mineral vector diagrams on Fig. 11a and b. The felsic rocks display a combined vector of potassium feldspar and plagioclase fractionation in Fig. 11a. Fig. 11b, however, shows that potassium feldspar fractionation was more important than plagioclase in controlling Ba abundances. Generally, negative Ti anomalies in all rocks (Fig. 7c and d) agree with fractionation of Fe–Ti oxides such as rutile and ilmenite.

The quartz monzonites and granites exhibit continuously decreasing Zr with increasing SiO2 (Fig. 5c), this indicates that zircon was saturated in the magma, which was also controlled by fractional crystallization (Li et al., 2007; Zhong et al., 2007). Zircon saturation thermometry (Watson and Harrison, 1983) provides a simple and robust means of estimating magma temperatures from bulk-rock compositions. The calculated zircon saturation temperatures (T_{Zr}) of the felsic rocks are 849–903 °C (Table 1), which represents the crystallization temperature of the magma. Moreover, the A-type granitoids show much higher values of zircon saturation temperatures (T_{Zr}) relative to the quartz monzonites.

5.1.4. Genetic model and process

There are various petrogenetic models for alkaline felsic rocks (e.g., syenites, A-type granites) (Yang et al., 2005a,b and the references therein; Zhong et al., 2007 and the references therein), including (1) partial melting of lower-crustal rocks under fluxing of volatiles; (2) fractionation of mantle derived magmas with or without crustal contamination; and (3) mixing of basic and silicic melts and their differentiates. Among them, the granitoids could be derived from dehydration melting of the lower crust (probably intermediate in composition in the North China Craton, Gao et al., 1998a,b) due to underplating of mantle-derived basaltic magmas. However, it is unlikely that the extensive melting of the lower crust can occur when basaltic melts underplate the lower crust (Defant et al., 2002). Moreover, the granitoids have relatively higher $\varepsilon_{Nd}(t)$ values than lower crustal values published for the North China Craton (Jahn et al., 1999), inconsistent with magma derivation directly from partial melting of lower crust. Otherwise, this model cannot give a reasonable interpretation for the absence of mafic lower crust underneath eastern China (Gao et al., 1998b). Furthermore, the insignificant variations of Sr–Nd isotopes with MgO for both the mafic and felsic rocks (Fig. 10) have eliminated the possibility of AFC process. Overall, we therefore propose fractionation of mantle derived magmas without interaction with crustal rocks as the best model for the origin of the quartz monzonites and A-type granites.

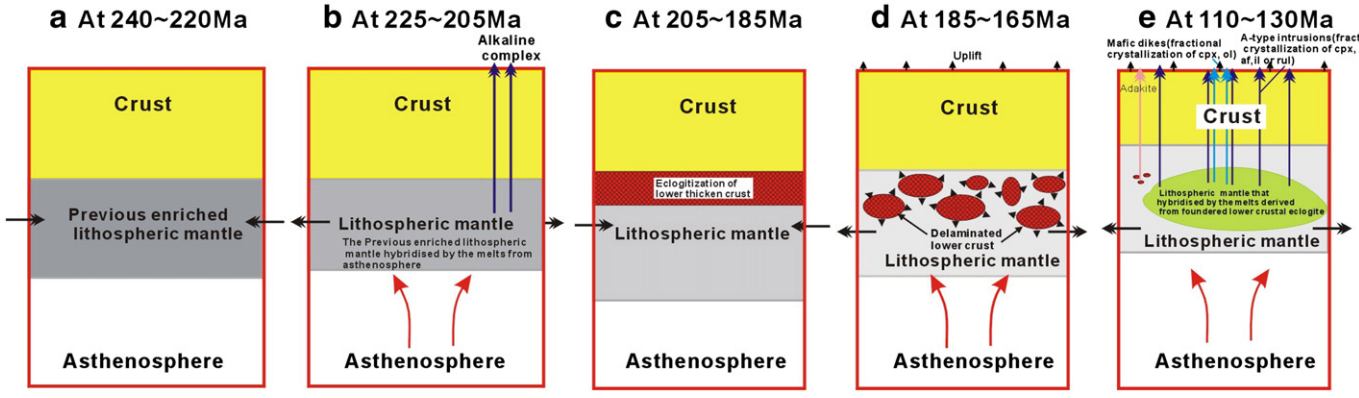

Fig. 12. Cartoon showing the lithospheric evolution and related magmatism beneath the Sulu belt. (a) At 240–220 Ma, a thick crust formed due to subduction between Yangtze Craton (YC) and North China Craton (NCC) (Guo et al., 2006 and the references therein), when enriched lithospheric mantle existed beneath the Sulu belt; (b) during 225–205 Ma (Chen et al., 2003), the breakoff of subducted Yangtze block induced asthenospheric upwelling, lithospheric extension, mantle hybridism and decompressional melting of enriched lithospheric mantle resulting in emplacement of alkaline magmas; (c) subsequent (205–185 Ma) compression between YC and NCC thickened the lithosphere and induced eclogitization of the lower crust; (d) for the higher density (relative to peridotite) eclogitized lower thicken crust foundered into lithospheric mantle between 185 and 165 Ma (Li et al., 2002), which triggered asthenospheric upwelling, orogenic collapse and lithospheric extension beneath the Sulu belt, as well as the reaction between mantle peridotite and melts from eclogites; (e) during the period of 127~114 Ma, decompressional melting of the hybridized lithospheric mantle produced primary magma (basaltic melts), subsequent magma fractionation occurred and formed the A-type intrusions and mafic dikes in this study (e). cpx— clinopyroxene; ol—olivine; pl—plagioclase; kf—potassium keldspar; Hb—hornblende; Bi—biotite, il—ilmenite; rul—rutile.

In the primitive mantle normalized diagrams (Fig. 7 c and d) all the rocks show very distinctive negative anomalies in HFSEs (Nb, Ta and Ti), and positive anomalies in Pb. HFSEs-depletion indicates the involvement of components from the proto-Tethyan oceanic or ancient continental crust (Zhang et al., 2005a,b). The higher La/Nb ratios (about 3–10) and Ba/Nb ratios (>50) in these rocks, however, are different from those of most intraplate volcanic rocks including N-MORB, OIB, alkali basalts and kimberlites with La/Nb ratios of 2.5 to 0.5 and much lower Ba/Nb ratios of 20 to 1 (Jahn et al., 1999). These suggest that continental materials (granitoids, granulites, sediments, etc.) were involved in these mantle-derived magmas, which is further supported by the low $\varepsilon_{Nd}(t)$ values from −15.3 to −19.2 and high $(^{87}Sr/^{86}Sr)_i$ (0.7079–0.7089) of the rocks (Table 2; Fig. 8), as well as the uniform zircon Hf isotopic compositions (Table 3 in the Appendix). The felsic rocks and mafic dikes share Pb isotopic characteristics (Table 2) different from those of the Yangtze craton lithosphere mantle (Yan et al., 2003; Fig. 9a, b), which rule out an involvement of Yangtze craton lithosphere. In summary, the parental magma of the felsic rocks and mafic dikes in this study were derived from melting of lithospheric mantle of North China Craton (NCC), and some ancient continental crust materials of NCC were involved during magma ascent by crustal contamination or in the source region due to metasomatism.

Based on the above interpretations, the possibility of crustal assimilation has been eliminated. Therefore, we prefer the involvement of crustal components in the source. Nevertheless, it is necessary to know by which mechanism the crustal materials sank into the lithospheric mantle. Foundering of continental lower crust into underlying convecting mantle has been proposed to play a role in plume magmatism, crustal evolution and formation of chemical heterogeneities within the mantle (Arndt and Goldstein, 1989; Kay and Kay, 1991; Rudnick and Fountain, 1995; Jull and Kelemen, 2001; Escrig et al., 2004; Gao et al., 2004; Elkins-Tanton, 2005; Lustrino, 2005; Anderson, 2006; Gao et al., 2008). This is due to the unique chemical and physical properties of eclogite formed by high to ultrahigh pressure metamorphism of basaltic rocks. Because of its higher density than that of lithospheric mantle peridotite by 0.2–0.4 g cm^{-3} (Rudnick and Fountain, 1995; Jull and Kelemen, 2001; Levander et al., 2006; Anderson, 2006), eclogite can be recycled into the mantle (Arndt and Goldstein, 1989; Kay and Kay, 1991; Jull and Kelemen, 2001; Gao et al., 2004). On the other hand, eclogites have lower melting temperatures than mantle peridotites (Yaxley and Green, 1998; Rapp et al., 1999; Yaxley, 2000; Kogiso et al., 2003; Sobolev et al., 2005, 2007), and as foundered, silica-saturated eclogites heat up, they will produce silicic melts (tonalite to trondhjemite) that may hybridize variably with overlying mantle peridotite. Such reaction may produce an olivine-free pyroxenite, which, if subsequently melted, will generate basaltic melt (Kogiso et al., 2003; Sobolev et al., 2005; Herzberg, 2006; Sobolev et al., 2007; Gao et al., 2008). The above model is ideal in explaining the mantle metasomatism, the origin of the primary magma of the rocks in this study and the production of adakitic lavas from foundered lower crust reported in the Sulu belt (Guo et al., 2006).

According to the above model, a scenario for the origin of the alkaline intrusions and mafic dikes in the Sulu belt is presented in Fig. 12. At ~240–220 Ma (Zhang et al., 2005a), the collision between the North China Craton and Yangtze Craton resulted in a thickened crust (Fig. 12a) and the peak metamorphism of HP–UHP terrane (Guo et al., 2006 and the references therein); At 225–205 Ma, the breakoff of the subducted Yangtze block occurred (Chen et al., 2003), together with convective removal of the lower lithospheric mantle (Yang et al., 2005a), inducing asthenospheric upwelling, lithospheric extension and emplacement of alkaline magmas (Fig. 12b), as well as the rapid exhumation of the UHP metamorphic terrane (Guo et al., 2006). Possibly, at 205–185 Ma, intracontinental compression between the NCC and Yangtze block further thickened the crust and induced eclogitization of the lower thickened crust (Fig. 12c). During 185–165 Ma, lithospheric delamination, mainly foundering of eclogites from lower thicken crust, occurred beneath the Dabie–Sulu orogenic belt (Li et al., 2002), which triggered asthenospheric upwelling, sudden uplift of the Sulu belt, orogenic collapse and lithospheric extension and thinning. Subsequently, silicic melts originated by melting of foundered eclogites which reacted extensively with the overlying mantle peridotite (Fig. 12d). Between 130–110 Ma (Li et al., 2002), decompressional melting of the hybridized lithospheric mantle produced primary magma (basaltic melts). Subsequently magma fractionation occurred and formed the A-type intrusions and mafic dikes (Fig. 12e). At ~114 Ma the eclogitic lower crust remaining from the delamination event was heated up in the lithospheric mantle and produced the adakitic lavas of the Sulu belt (Guo et al., 2006; Fig. 12e).

5.2. Tectonic significance

It is believed that alkaline intrusions (e.g., Whalen et al., 1987; Sylvester, 1989; Eby, 1992; Shao et al., 2000;Yan et al., 2000; Wu et al., 2002; Chen et al., 2003; Zhang et al., 2005b; Yang et al., 2005a,b; Xie et al., 2006; Ying et al., 2007; Li et al., 2007; Zhong et al., 2007) and mafic dikes (e.g., Hall, 1982; Hall and Fahrig, 1987; Tarney and Weaver, 1987; Zhao and McCulloch, 1993; Shao and Zhang, 2002; Liu et al., 2004, 2006) are mostly emplaced in extensional tectonic settings. Various tectonic models now have been proposed for the Mesozoic magmatism and crustal extension in the eastern China. For example, Chen et al. (2004) concluded that all Mesozoic magmatism in eastern China was developed in a back-arc extensional setting due to the subduction of Paleo-Pacific slab (Izanagi plate) beneath the East Asian continent. However, the late Mesozoic was a period when the Izanagi plate primarily moved toward the north or north–northeast, thus giving little chance for inducing broad back arc extension in this region (Maruyama and Send, 1986; Kimura et al., 1990; Ying et al., 2007). An alternative possibility is lithospheric thinning and crustal extension induced by convective instability of a thickened mantle boundary layer (Houseman et al., 1981). Accordingly, the removal of the lower continental lithospheric mantle has been considered as a possible model for interpreting the origin of Jiazishan complex in the Sulu orogenic belt (Yang et al., 2005a,b). Based on the above interpretations, foundering of lower crust may play an important role in the lithospheric extension. However, the absence of magmatism between 185 and 165 Ma in the Sulu belt (Zhao et al., 1997; Zhou and Lu, 2000; Fan et al., 2001; Chen et al., 2003; Zhou et al., 2003; Guo et al., 2004, 2005; Huang et al., 2005; Meng et al., 2005; Yang et al., 2005a,b; Guo et al., 2006) argues against its effect on magmatic activity. Overall, the voluminous magmatism in the Sulu belt (Fig. 12e) might be related to foundering of lower lithosphere (mantle and lower crust) between 130 and 110 Ma (Li et al., 2002).

Since the 1980s, Phanerozoic lithosphere removal beneath eastern China has been recognized (Chi, 1988; Menzies et al., 1993; Deng et al., 1994, 1996; Menzies and Xu, 1998; Griffin et al., 1998; Zheng, 1999; Wu and Sun, 1999; Fan et al., 2000; Wu et al., 2000; Xu, 2001; Gao et al., 2002; Wu et al., 2003a,b). The exact time and mechanism of lithospheric thinning, however, remains controversial. Based on previous studies, Wu et al. (2003a) proposed that late Mesozoic between 130 and 120 Ma is a peak of lithospheric removal beneath eastern China. Theoretically, lithospheric foundering would result in lithospheric thinning and coeval magmatism (Kay and Kay, 1993). According to the above discussions, magmatic activities in the Sulu belt mostly occurred between 130 and 110 Ma. We thus suggest that 130–110 Ma is a dominant period for the lithospheric removal beneath the Sulu orogenic belt. Potentially, thermo-chemical erosion of the Archean lithospheric mantle by upwelling asthenosphere (Menzies et al., 1993; Griffin et al., 1998; Menzies et al., 2007) or transformation of lithospheric to asthenospheric mantle by addition of melts (Zhang et al., 2007) or melts and water from a subducting slab (Niu, 2005) are possible mechanisms for the destruction of the NCC Archean keel. None of these processes, however, can explain the production of adakitic lavas from foundered lower crust,

as observed in the Chuzhou lavas from the Sulu belt (Guo et al., 2006). Therefore, we propose that lithospheric thinning underneath the Sulu belt of eastern China was caused by the removal of the lower lithosphere (mantle and lower crust).

6. Conclusions

Based on the geochronological, geochemical and Sr–Nd–Pb–Hf isotopic studies, we draw the following conclusions:

(1) SHRIMP U–Pb zircon dating results indicate that the alkaline quartz monzonites, granites and associated mafic dikes were formed between 119.0±1.7 Ma and 126.9±1.9 Ma. These rocks are all the results of post-orogenic magmatism.
(2) The felsic rocks and mafic dikes resulted from a common source. The parental magma originated by partial melting of an enriched lithospheric mantle beneath the Sulu belt due to hybridization of melts derived from foundered lower crustal eclogites. Subsequent fractionation of olivine, clinopyroxene, K-feldspar, plagioclase and ilmenite or rutile resulted in the alkaline association with negligible crustal contamination. The zircon saturation temperatures (T_{Zr}) of the felsic rocks are 849–903 °C, which approximately represents the crystallization temperature of the magma.
(3) It is proposed that intense lithospheric thinning beneath the Sulu belt of eastern China occurred between 110 and 130 Ma due to the foundering of the lower lithosphere (mantle and lower crust).

Acknowledgements

The authors would like to thank G. Nelson Eby and two anonymous reviewers for their constructive reviews of this manuscript. This research was supported by Chinese 973 program (2007CB411402), the Knowledge innovation project (KZCX2-YW-111-03), National 305 project (2006BAB07B04-04) and the National Nature Science Foundation of China (40673029, 40773020, 90714010, 40634020). We are grateful to Gui-xiang Yu for helping analyze Sr, Nd and Pb isotopes, and Lie-wen Xie, Yan-bin, Zhang, Yue-heng Yang for help in Hf isotopic analysis. Yu-Ruo Shi and Hang-qiang Xie are thanked for help with SHRIMP dating. Thanks are also due to Shandong Provincial Department of Land and Resources for providing some regional geologic data.

Appendix A. Supplementary data

Supplementary data associated with this article can be found, in the online version, at doi:10.1016/j.lithos.2008.09.004.

References

Anderson, D.A., 2006. Speculations on the nature and cause of mantle heterogeneity. Tectonophysics 146, 7–22.
Arndt, N.T., Goldstein, S.L., 1989. An open boundary between lower continental crust and mantle: its role in crust formation and crustal recycling. Tectonophysics 161, 201–212.
Bacon, C.R., Druitt, T.H., 1988. Compositional evolution of the zoned calcalkaline magma chamber of Mount-Mazama, Crater Lake, Oregon. Contributions to Mineralogy and Petrology 98, 224–256.
Barry, T.L., Kent, R.W., 1998. Cenozoic magmatism in Mongolia and the origin of central and east Asian basalts. In: Flower, M.F.J., Chung, S.L., Lo, C.H., Lee, T.Y. (Eds.), Mantle Dynamics and Plate Interactions in East Asia. American Geophysical Union—Geodynamics Series, vol. 27, pp. 347–364.
Black, L.P., Kamo, S.L., Allen, C.M., Aleinikoff, J.N., Davis, D.W., Korsch, R.J., Foudoulis, C., 2003. TEMORA 1: a new zircon standard for Phanerozoic U–Pb geochronology. Chemical Geology 200, 155–170.
Blichert-Toft, J., Albare'de, F., 1997. The Lu–Hf geochemistry of chondrites and the evolution of the mantle–crust system. Earth and Planetary Science Letters 148, 243–258.
Bonin, B., Platevoet, B., Vialette, Y., 1987. The geodynamic significance of alkaline magmatism in the Western Mediterranean compared with West Africa. In: Bowden, P., Kinnaird, J. (Eds.), African Geology Reviews. Geological Journal, vol. 22, pp. 361–387.
Bureau of Geology and Mineral Resources of Shandong Province (BGMRS), 1991a. Attached map 2 of Regional geology of Shandong Province. Geological Publishing House, Beijing. (in Chinese).
Bureau of Geology and Mineral Resources of Shandong Province (BGMRS), 1991b. Regional Geology of Shandong Province. Geological Publishing House, Beijing. (594 pp., in Chinese).
Cao, G., Wang, Z., Zhang, C., 1990. The Jiaonan terrane in Shandong Province and the tectonic significance of Wulian–Rongcheng fault. Shandong Geology 6, 1–15 (in Chinese).
Chen, B., Jahn, B.M., Arakawa, A., Zhai, M.G., 2004. Petrogenesis of the Mesozoic intrusive complexes from the southern Taihang Orogen, North China Craton and Sr-Nd-Pb isotopic constraints. Contributions to Mineralogy and Petrology 148, 489–501.
Chen, J.F., Xie, Z., Li, H.M., Zhang, X.D., Zhou, T.X., Park, Y.S., Ahn, K.S., Chen, D.G., Zhang, H., 2003. U–Pb zircon ages for a collision-related K-rich complex at Shidao in the Sulu ultrahigh pressure terrane, China. Chemical Geology 37, 35–46.
Cheng, X., Cheng, J., Wang, J., 1998. Element geochemistry of shoshonitic lamprophyres in the Pengjiakuang gold district, Shandong Province, China. Geochimica 27, 91–100 (in Chinese with English abstract).
Chi, J.S., 1988. Research on the Cenozoic Basalts and Upper Mantle, Eastern China. Publishing House of China University of Geosciences, Wuhan. (in Chinese).
Compston, W., Williams, I.S., Kirschvink, J.L., Zhang, Z., Ma, G., 1992. Zircon U–Pb ages fro the Early Cambrian time-scale. The Geological Society of London 149, 171–184.
Cong, B.L. (Ed.), 1996. Ultrahigh-Pressure Metamorphic Rocks in the Dabie–Sulu Region of China. Science Press. Beijing: China and Kluwer Academic Publishing, Dordrecht, 224 pp.
Currie, K.L., 1970. A hypothesis on the origin of alkaline rocks suggested by the tectonic setting of the Montere. Canada Mineralogist 10, 411–420.
Defant, M.J., Kepezhinskas, P., Defant, M.J., Xu, J.F., Kepezhinskas, P., Wang, Q., Zhang, Q., Xiao, L., 2002. Adakites: some variations on a theme. Acta Petrologica Sinica 18, 129–142.
Deng, J.F., Mo, X.X., Zhao, H.L., Luo, Z.H., Du, Y.S., 1994. Lithosphere root/de-rooting and activation of the east China continent. Geoscience 8, 349–356 (in Chinese with English abstract).
Deng, J.F., Zhao, H.L., Mo, X.X., 1996. Continental Roots-Plume Tectonics of China—Key to the Continental Dynamics. Geological Publishing House, Beijing. (in Chinese).
DePaolo, D.J., 1981. Trace element and isotopic effects of combined wallrock assimilation and fractionation crystallization. Earth and Planetary Science Letters 53, 189–202.
Devey, C.W., Cox, K.G., 1987. Relationships between crustal contamination and crystallization in continental flood basalt magmas with special reference to the Deccan Traps of the Western Ghats, India. Earth and Planetary Science Letters 84, 59–68.
Eby, G.N., 1992. Chemical subdivision of the A-type granitoids: petrogenetic and tectonic implications. Geology 20, 641–644.
Elkins-Tanton, L.T., 2005. Continental magmatism caused by lithospheric delamination. In: Foulger, G.R., Natland, J.H., Presnall, D.C., Anderson, D.L. (Eds.), Plates, Plumes, and Paradigms. Geological Society of London Special Publication, vol. 388, pp. 449–462.
Escrig, S., Capmas, F., Dupré, B., Allégre, C.J., 2004. Osmium isotopic constraints on the nature of the DUPAL anomaly from Indian mid-ocean-ridge basalts. Nature 431, 59–63.
Fan, W.M., Zhang, H.F., Baker, J., Javis, K.E., Mason, P.R.D., Menzies, M.A., 2000. On and off the North China craton: where is the Archean keel? Journal of Petrology 41, 933–950.
Fan, W.M., Guo, F., Wang, Y.J., Lin, G., Zhang, M., 2001. Postorogenic bimodal volcanism along the Sulu orogenic belt in eastern China. Physics and Chemistry of the Earth (A) 26, 733–746.
Gao, S., Luo, T.-C., Zhang, B.-R., Zhang, H.-F., Han, Y.-W., Zhao, Z.-D., Hu, Y.-K., 1998a. Chemical composition of the continental crust as revealed by studies in East China. Geochimica et Cosmochimica Acta 62, 1959–1975.
Gao, S., Zhang, B.-R., Jin, Z.-M., Kern, H., Luo, T.-C., Zhao, Z.-D., 1998b. How mafic is the lower continental crust? Earth and Planetary Science Letters 106, 101–117.
Gao, S., Rudnick, R.L., Carlson, R.W., McDonough, W.F., Liu, Y.S., 2002. Re–Os evidence for replacement of ancient mantle lithosphere beneath the North China Craton. Earth and Planetary Science Letters 198, 307–322.
Gao, S., Rudnick, R.L., Yuan, H.-L., Liu, X.-M., Liu, Y.-S., Xu, W.-L., Ling, W.-L., Ayers, J., Wang, X.-C., Wang, Q.-H., 2004. Recycling lower continental crust in the North China craton. Nature 432, 892–897.
Gao, S., Rudnick, R.L., Xu, W.L., Yuan, H.L., Liu, Y.S., Walker, R.J., Puchtel, I., Liu, X.M., Huang, H., Wang, X.R., Yang, J., 2008. Recycling deep cratonic lithosphere and generation of intraplate magmatism in the North China Craton. Earth and Planetary Science Letters 270, 41–53.
Goolaerts, A., Mattielli, N., de Jong, J., Weis, D., Scoates, J.S., 2004. Hf and Lu isotopic reference values for the zircon standard 91500 by MC-ICP-MS. Chemical Geology 206, 1–9.
Griffin, W.L., Zhang, A., O'Reilly, S.Y., Ryan, C.G., 1998. Phanerozoic evolution of the lithosphere beneath the Sino-Korean Craton. Mantle dynamics and plate interaction in East Asia. In: Flower, M.F.J., Chung, S.L., Lo, C.H., Lee, T.Y. (Eds.), Geodynamic Series. American Geophysical Union, Washington, D.C., pp. 107–126.
Griffin, W.L., Pearson, N.J., Belousova, E., Jackson, S.E., van Achterbergh, E., O'Reilly, S.Y., Shee, S.R., 2000. The Hf isotope composition of cratonic mantle: LAM-MC-ICPMS analysis of zircon megacrysts in kimberlites. Geochimica et Cosmochimica Acta 4, 133–147.
Guo, F., Fan, W.M., Wang, Y.J., Zhang, M., 2004. Origin of early Cretaceous calc-alkaline lamprophyres from the Sulu orogen in eastern China: implications for enrichment processes beneath continental collisional belt. Lithos 78, 291–305.
Guo, J.H., Chen, F.K., Zhang, X.M., Siebel, W., Zhai, M.G., 2005. Evolution of syn- to post-collisional magmatism from north Sulu UHP belt, eastern China: zircon U–Pb geochronology. Acta Petrologica Sinica 21, 1281–1301.
Guo, F., Fan, W.M., Li, C.W., 2006. Geochemistry of late Mesozoic adakites from the Sulu belt, eastern China: magma genesis and implications for crustal recycling beneath continental collisional orogens. Geological Magazine 143, 1–13.

Hall, H.C., 1982. The importance and potential of mafic dyke swarms in studies of geodynamic process. Geosciences in Canada 9, 145–154.
Hall, H.C., Fahrig, W.F., 1987. Mafic dyke swarms. Geological Association of Canada Special Paper 34, 1–503.
Harris, N.B.W., 1985. Alkaline complexes from the Arabian Shield. In: Black, R., Bowden, P. (Eds.), Alkaline Ring Complexes in Africa. Journal of African Earth Sciences, vol. 3, pp. 3–88.
Hart, S.R., 1984. A large-scale isotope anomaly in the Southern Hemisphere mantle. Nature 309, 753–757.
Herzberg, C., 2006. Petrology and thermal structure of the Hawaiian plume from Mauna Kea volcano. Nature 444, 605–609.
Hirajima, T., Ishiwatari, A., Cong, B., Zhang, R., Banno, S., Nozaka, T., 1990. Coesite from Mengzhong eclogite at Donghai county, northern Jiangsu province, China. Mineralogy Magazine 54, 579–583.
Hong, D.W., Wang, T., Tong, Y., Wang, X.X., 2003. Mesozoic granitoids from North China Block and Qinling–Dabie–Sulu orogenic belt and their deep dynamic process. Earth Science Frontiers 10, 231–256.
Houseman, G.A., McKenzie, D.P., Molnar, P., 1981. Convective instability of a thickened boundary layer and its relevance for the thermal evolution of continental convergent belts. Journal of Geophysical Research 86, 6115–6132.
Huang, J., Zheng, Y.F., Wu, Y.B., Zhao, Z.F., 2005. Geochemistry of elements and isotopes in igneous rocks from the Wulian region in the Sulu orogen. Acta Petrologica Sinica 21, 545–568.
Jahn, B.M., Cornichet, J., Cong, B.L., Yui, T.F., 1996. Ultrahigh-ε_{Nd} eclogites from an ultrahigh-pressure metamorphic terrane of China. Chemical Geology 127, 61–79.
Jahn, B.M., Wu, F.Y., Lo, C.H., Tsai, C.H., 1999. Crustmantle interaction induced by deep subduction of the continental crust: geochemical and Sr–Nd isotopic evidence from post-collisional mafic–ultramafic intrusions of the northern Dabie complex, central China. Chemical Geology 157, 119–146.
Jull, M., Kelemen, P.B., 2001. On the conditions for lower crustal convective instability. Journal of Geophysical Research 106, 6423–6446.
Kato, T., Enami, A., Zhai, M., 1997. Ultrahigh-pressure marble and eclogite in the Su-Lu ultrahigh-pressure terrane, eastern China. Journal of Metamorphic Geology 15, 169–182.
Kay, R.W., Kay, S.M., 1991. Creation and destruction of lower continental crust. Geologische Rundschau 80, 259–278.
Kay, R.W., Kay, S.M., 1993. Delamination and delamination magmatism. Tectonophysics 219, 177–189.
Kimura, G., Takahashi, M., Kono, M., 1990. Mesozoic collision extrusion tectonics in eastern Asia. Tectonophysics 181, 15–23.
Kogiso, T., Hirschmann, M.M., Frost, D.J., 2003. High-pressure partial melting of garnet pyroxenite: possible mafic lithologies in the source of ocean island basalts. Earth and Planetary Science Letters 216, 603–617.
Le Maitre, R.W., 2002. Igneous Rocks: A Classification and Glossary of Terms, 2nd. Cambridge University Press, Cambridge. 236 pp.
Levander, A., Niu, F., Lee, C.T.A., Cheng, X., 2006. Imaging the continental lithosphere. Tectonophysics 416, 167–185.
Li, S.G., Huang, F., Li, H., 2002. Post-collisional delamination of the lithosphere beneath Dabie–Sulu orogenic belt. Chinese Science Bulletin 46, 1487–1490.
Li, S.G., Jagoutz, E., Lo, C.-H., Chen, Y.Z., Li, Q.L., 1999. Sm/Nd, Rb/Sr and $^{40}Ar/^{39}Ar$ isotopic systematics of the ultrahigh-pressure metamorphic rocks in the Dabie– Sulu belt central China: a retrospective view. International Geology Review 41, 1114–1124.
Li, X.H., Li, Z.X., Li, W.X., Liu, Y., Yuan, C., Wei, G.J., Qi, C.S., 2007. U–Pb zircon, geochemical and Sr–Nd–Hf isotopic constraints on age and origin of Jurassic I- and A-type granites from central Guangdong, SE China: a major igneous event in response to foundering of a subducted flat-slab? Lithos 96, 186–204.
Lin, J.Q., Tan, D.J., Chi, X.G., Bi, L.J., Xie, C.F., Xu, W.L., 1992. Mesozoic Granites in Jiao-Liao Peninsula. Science Press, Beijing, p. 208 (in Chinese with English abstract).
Liu, S., Hu, R.Z., Zhao, J.H., Feng, C.X., 2004. K–Ar Geochronology of Mesozoic mafic dikes in Shandong Province, Eastern China: implications for crustal extension. Acta Geologica Sinica 78, 1207–1213.
Liu, S., Zou, H.B., Hu, R.Z., Zhao, J.H., Feng, C.X., 2006. Mesozoic mafic dikes from the Shandong Peninsula, North China Craton: petrogenesis and tectonic implications. Geochemical Journal 40, 181–195.
Iizuka, T., Hirata, T., 2005. Improvements of precision and accuracy in in situ Hf isotope microanalysis of zircon using the laser ablation–MC-ICPMS technique. Chemical Geology 220, 121–137.
Lugmair, G.W., Harti, K., 1978. Lunar initial $^{143}Nd/^{144}Nd$: differential evolution of the lunar crust and mantle. Earth and Planetary Science Letters 39, 349–357.
Lustrino, M., 2005. How the delamination and detachment of lower crust can influence basaltic magmatism. Earth-Science Reviews 72, 21–38.
Marsh, J.S., 1989. Geochemical constraints on coupled assimilation and fractional crystallization involving upper crustal compositions and continental tholeiitic magma. Earth Planetary Science Letter 92, 78–80.
Maruyama, S., Send, T., 1986. Orogeny and relative plate motions: example of the Japanese Islands. Tectonophysics 127, 305–329.
Meng, F.C., Xue, H.M., Li, T.F., Yang, H.R., Liu, F.L., 2005. Enriched characteristics of Late Mesozoic mantle under the Sulu orogenic belt: geochemical evidence from gabbro in Rushan. Acta Petrologica Sinica 21, 1583–1592.
Menzies, M.A., Kyle, P.R., 1990. Continental volcanism: a crust–mantle probe. In: Menzies, M.A. (Ed.), Continental Mantle. Oxford University Press, Oxford, pp. 157–177.
Menzies, M.A., Xu, Y.G., 1998. Geodynamics of the North China Craton. In: Flower, M., Chung, S.L., Lo, C.H., Lee, T.Y. (Eds.), Mantle Dynamics and Plate Interactions in East Asia. American Geophysical Union Geodynamics Series, vol. 27, p. 155.
Menzies, M.A., Fan, W.M., Zhang, M., 1993. Paleozoic and Cenozoic lithoprobes and loss of >120 km of Archean lithosphere, Sino-Korean Craton, China, magmatic processes and plate tectonics. Geological Society of London Special Publication. Academic Press, London.
Menzies, M.A., Xu, Y., Zhang, H., Fan, W., 2007. Integration of geology, geophysics and geochemistry: a key to understanding the North China Craton. Lithos 96, 1–21.
Middlemost, E.A.K., 1972. A simple classification of volcanic rocks. Bulletin of Volcanology 36, 382–397.
Middlemost, E.A.K., 1994. Naming materials in the magma/igneous rock system. Earth-Science Reviews 74, 193–227.
Miller, C., Schuster, R., Klötzli, U., Frank, W., Purtscheller, F., 1999. Post-collisional potassic and ultrapotassic magmatism in SW Tibet: geochemical and Sr–Nd–Pb–O isotopic constraints for mantle source characteristics and petrogenesis. Journal of Petrology 40, 1399–1424.
Mingram, B., Trumbull, R.B., Littman, S., Gertenberger, H., 2000. A petrogenetic study of anorogenic felsic magmatism in the Cretaceous Paresis ring complex, Namibia: evidence for mixing of crust and mantle-derived components. Lithos 54, 1–22.
Niu, Y.L., 2005. Generation and evolution of basaltic magmas: some basic concepts and a new view on the origin of Mesozoic-Cenozoic basaltic volcanism in Eastern China. Geological Journal of China Universities 11, 9–46.
Philpotts, J.A., Schnetzler, C.C., 1970. Phenocryst–matrix partition coefficients for K, Rb, Sr and Ba, with applications to anorthosite and basalt genesis. Geochimica et Cosmochimica Acta 34, 307–322.
Potts, P.J., Kane, J.S., 2005. International association of geoanalysts certificate of analysis: certified reference material OU-6 (Penrhyn slate). Geostandards and Geoanlytical Research 29, 233–236.
Qi, L., Hu, J., Grégoire, D.C., 2000. Determination of trace elements in granites by inductively coupled plasma mass spectrometry. Talanta 51, 507–513.
Rapp, R.P., Shimizu, N., Norman, M.D., Applegate, G.S., 1999. Reaction between slab-derived melts and peridotite in the mantle wedge: experimental constraints at 3.8 GPa. Chemical Geology 160, 335–356.
Rapp, R.P., Shimizu, N., Norman, M.D., 2003. Growth of early continental crust by partial melting of eclogite. Nature 425, 605–609.
Ren, K.X., 2003. Study progress of the alkaline rocks: a review. Geology of Chemical Minerals 25, 151–163 (in Chinese with English abstract).
Rudnick, R.L., Fountain, D.M., 1995. Nature and composition of the continental crust: a lower crustal perspective. Reviews of Geophysics 33, 267–309.
Schnetzler, C.C., Philpotts, J.A., 1970. Partition coefficients of rare-earth elements between igneous matrix material and rock-forming mineral phenocrysts; II. Geochimica et Cosmochimica Acta 34, 331–340.
Shao, J.A., Zhang, L.Q., 2002. Mesozoic dyke swarms in the north of North China. Acta Petrologica Sinica 18, 312–318.
Shao, J.A., Mu, B.L., Zhang, L., 2000. Deep geological process and its shallow response during Mesozoic transfer of tectonic framework in eastern North China. Geological Review 46, 32–40 (in Chinese with English abstract).
Sobolev, A.V., Hofmann, A.W., Sobolev, S.V., Nikogosian, I.K., 2005. An olivine-free mantle source of Hawaiian shield basalts. Nature 434, 590–597.
Sobolev, A.V., et al., 2007. The amount of recycled crust in sources of mantle-derived melts. Science 316, 412–417.
Soderlund, U., Patchett, P.J., Vervoort, J.D., Isachsen, C.E., 2004. The ^{176}Lu decay constant determined by Lu–Hf and U–Pb isotope systematics of Precambrian mafic intrusions. Earth and Planetary Science Letters 219, 311–324.
Song, B., Zhang, Y.H., Wan, Y.S., Jian, P., 2002. Mount Making and procedure of the SHRIMP dating. Geological Review 48, 26–30 (Suppl., in Chinese).
Steiger, R.H., Jäger, E., 1977. Subcommission on geochronology; convention on the use of decay constants in geochronology and cosmochronology. Earth and Planetary Science Letters 36, 359–362.
Sun, S.S., McDonough, W.F., 1989. Chemical and isotopic systematics of oceanic basalts: implications for mantle composition and processes. In: Saunders, A.D., Norry, M.J. (Eds.), Magmatism in the Ocean Basins. Geological Society Special Publication, London, pp. 313–345.
Sylvester, P.J., 1989. Post-collisional alkaline granites. Journal of Geology 97, 261–280.
Tarney, J., Weaver, B.L., 1987. Geochemistry and petrogenesis of Early Proterozoic dyke swarms. In: Halls, H.C., Fahrig, W.C. (Eds.), Mafic Dyke Swarms. Special Publication—Geological Association of Canada, vol. 34, pp. 81–93.
Thompson, M., Potts, P.J., Kane, J.S., Wilson, S., 2000. An International Proficiency Test for Analytical Geochemistry Laboratories—Report on Round 5 (August 1999). Geostandards and Geoanlytical Research 24, E1–E28.
Turner, S., Arnaud, N., Liu, J., Rogers, N., Hawkesworth, C., Harris, N., Kelley, S., Van Calsteren, P., Deng, W., 1996. Postcollision, shoshonitic volcanism on the Tibetan Plateau: implications for convective thinning of the lithosphere and the source of ocean island basalts. Journal of Petrology 37, 45–71.
Wang, Y.M., Gao, Y.S., Han, H.M., Wang, X.H., 2003. Practical Handbook of Reference Materials for Geoanalysis. Geological Publishing House. (in Chinese).
Watson, E.B., Harrison, T.M., 1983. Zircon saturation revisited: temperature and composition effects in a variety of crustal magma types. Earth and Planetary Science Letters 64, 295–304.
Whalen, J.B., Currie, K.L., Chappell, B.W., 1987. A-type granites: geochemical characteristics, discrimination and petrogenesis. Contributions to Mineralogy and Petrology 95, 407–419.
Williams, I.S., 1998. U–Th–Pb geochronology by ion microprobe. In: McKibben, M.A., ShanksIII III, W.C., Ridley, W.I. (Eds.), Applications of Microanalytical Techniques to Understanding Mineralizing Processes. Reviews of Economic Geology, vol. 7, pp. 1–35.
Williams, H.M., Turner, S.P., Pearce, J.A., Kelley, S.P., Harris, N.B.W., 2004. Nature of the source regions for post-collisional, potassic magmatism in southern and northern Tibet from geochemical variations and inverse trace element modelling. Journal of Petrology 45, 555–607.
Woodhead, J., Hergt, J., Shelley, M., Eggins, S., Kemp, R., 2004. Zircon Hf-isotope analysis with an excimer laser, depth profiling, ablation of complex geometries, and concomitant age estimation. Chemical Geology 209, 121–135.

Wu, F.Y., Sun, D.Y., 1999. The Mesozoic magmatism and lithospheric thinning in eastern China. Journal of Changchun University of Science and Technology 29, 313–318 (in Chinese).
Wu, F.Y., Sun, D.Y., Zhang, G.L., 2000. Deep geodynamics of Yanshan movement. Journal of China University of Geosciences 6, 379–388 (in Chinese).
Wu, F.Y., Sun, D.Y., Li, H.M., Jahn, B.M., Wilde, S., 2002. A-type granites in northeastern China: age and geochemical constraints on their petrogenesis. Chemical Geology 187, 143–173.
Wu, F.Y., Ge, W.C., Sun, D.Y., Guo, C.L., 2003a. Discussions on the lithospheric thinning in eastern China. Earth Science Frontiers 10, 51–60 (in Chinese with English abstract).
Wu, F.Y., Walker, R.J., Ren, X.W., Sun, D.Y., Zhou, X.H., 2003b. Osmium isotopic constraints on the age of lithospheric mantle beneath northeastern China. Chemical Geology 196, 107–129.
Wu, F.Y., Yang, Y.H., Xie, L.W., Yang, J.H., Xu, P., 2006. Hf isotopic compositions of the standard zircons and baddeleyites used in U–Pb geochronology. Chemical Geology 234, 105–126.
Xie, Z., Li, Q.Z., Gao, T.S., 2006. Comment on "Petrogenesis of post-orogenic syenites in the Sulu orogenic belt, east China: Geochronological, geochemical and Nd–Sr isotopic evidence" by Yang et al. Chemical Geology 235, 191–194.
Xu, Y.G., 2001. Thermo-tectonic destruction of the Archaean lithospheric keel beneath eastern China: evidence, timing and mechanism. Physics and Chemistry of the Earth 26, 747–757.
Xu, J.W., Zhu, G., 1994. Tectonic models of the Tan-Lu fault zone, eastern China. International Geology Review 36, 771–784.
Xu, P., Wu, F.Y., Xie, L.W., Yang, Y.H., 2004. Hf isotopic compositions of the standard zircons for U–Pb dating. Chinese Science Bulletin 49, 1642–1648.
Yan, G.H., et al., 2000. Geochronology and isotopic features of Sr, Nd, and Pb of the Triassic alkali intrusions in the Yanshan–Yinshan regions. Science in China. Series D, Earth Science 30, 384–387.
Yan, G.H., Mou, B.L., Xu, B.L., 2002. Geochronology and Nd–Sr–Pb isotopic characteristics of the Phanerozoic alkali—rich intrusive rocks in northern China and their implications. Geological Review 48 (Sup1), 69–75 (in Chinese with English abstract).
Yan, J., Chen, J.F., Yu, G., Qian, H., Zhou, T.X., 2003. Pb isotopic characteristics of Late Mesozoic mafic rocks from the Lower Yangtze Region: evidence for enriched mantle. Journal of China University of Geosciences 9, 195–206 (in Chinese).
Yang, J.H., Zhou, X.H., 2001. Rb–Sr, Sm–Nd, and Pb isotope systematics of pyrite: implications for the age and genesis of lode gold deposits. Geology 29, 711–714.
Yang, J., Godard, G., Kienast, J.R., Lu, Y., Sun, J., 1993. Ultrahigh pressure 60 kbar magnesite-bearing garnet peridotites from northeastern Jiangsu, China. Journal of Geology 101, 541–554.
Yang, J.H., Chung, S.L., Wilde, S.A., Wu, F.Y., Chu, M.F., Lo, C.H., Fan, H.R., 2005a. Petrogenesis of post-orogenic syenites in the Sulu Orogenic Belt, East China: geochronological, geochemical and Nd–Sr isotopic evidence. Chemical Geology 214, 99–125.
Yang, J.H., Wu, F.Y., Chung, S.L., Wilde, S.A., Chu, M.F., Lo, C.H., Song, B., 2005b. Petrogenesis of Early Cretaceous intrusions in the Sulu ultrahigh-pressure orogenic belt, east China and their relationship to lithospheric thinning. Chemical Geology 222, 200–231.
Yaxley, G.M., 2000. Experimental study of the phase and melting relations of homogeneous basalt plus peridotite mixtures and implications for the petrogenesis of flood basalts. Contributions to Mineralogy and Petrology 139, 326–338.
Yaxley, G.M., Green, D.H., 1998. Reactions between eclogite and peridotite: mantle refertilisation by subduction of oceanic crust. Schweizerische Mineralogische und Petrographische Mitteilungen 78, 243–255.
Ye, K., Hirajima, T., Ishiwateri, A., 1996. Significance of interstitial coesite in eclogites from Yankou, Qingdao city, eastern China. Chinese Science Bulletin 41, 1047–1048 (in Chinese).
Ye, K., Ye, D.N., Cong, B.L., 2000. The possible subduction of continental material to depths greater than 200 km. Nature 407, 734–736.
Yin, A., Ni, S., 1993. An indentation model for the north and south China collision and the development of the Tan-Lu and Honam fault systems, eastern Asia. Tectonics 124, 801–813.
Ying, J.F., Zhang, H.F., Sun, M., Tang, Y.J., Zhou, X.H., Liu, X.M., 2007. Petrology and geochemistry of Zijinshan alkaline intrusive complex in Shanxi Province, western North China Craton: implication for magma mixing of different sources in an extensional regime. Lithos 98, 45–66.
Zhai, M.G., Cong, B.L., Guo, J.H., Liu, W.J., Li, Y.G., Wang, Q.C., 2000. Division of petrological–tectonic units in the northern Sulu ultrahigh-pressure zone: an example of thick-skin thrust of crystalline units. Acta Geologica Sinica 35, 16–26 (in Chinese with English abstract).
Zhang, R.Y., Liou, J.G., Cong, B., 1994. Petrogenesis of garnet bearing ultramafic rocks and associated eclogites in the Sulu ultrahigh-P metamorphic terrane, eastern China. Journal of Metamorphic Geology 12, 169–186.
Zhang, R.Y., Hirajima, T., Banno, S., Cong, B., Liou, J.G., 1995. Petrology of ultrahigh-pressure metamorphic rocks in southern Sulu region, eastern China. Journal of Metamorphic Geology 13, 659–675.
Zhang, H.F., Sun, M., Zhou, M.F., Fan, W.M., Zhou, X.H., Zhai, M.G., 2004. Highly heterogeneous Late Mesozoic lithospheric mantle beneath the North China Craton: evidence from Sr–Nd–Pb isotopic systematics of mafic igneous rocks. Geological Magazine 141, 55–62.
Zhang, H.F., Sun, M., Zhou, X.H., Ying, J.F., 2005a. Geochemical constraints on the origin of Mesozoic alkaline intrusive complexes from the North China Craton and tectonic implications. Lithos 81, 297–317.
Zhang, H.F., Zhou, X.H., Fan, W.M., Sun, M., Guo, F., Ying, J.F., Tang, Y.J., Zhang, J., Niu, L.F., 2005b. Nature, composition, enrichment processes and its mechanism of the Mesozoic lithospheric mantle beneath the southeastern North China Craton. Acta Petrologica Sinica 21, 1271–1280.
Zhang, H.F., Ying, J.F., Shimoda, G., Kita, N.T., Morishita, Y., Shao, J.-A., Tang, Y.-J., 2007. Importance of melt circulation and crust–mantle interaction in the lithospheric evolution beneath the North China Craton: evidence from Mesozoic basalt-borne clinopyroxene xenocrysts and pyroxenite xenoliths. Lithos 96, 67–89.
Zhao, J.X., McCulloch, M.T., 1993. Melting of a subduction-modified continental lithospheric mantle: evidence from late Proterozoic mafic dike swarms in central Australia. Geology 21, 463–466.
Zhao, G., Wang, D., Cao, Q., 1997. Geochemical features and petrogenesis of Laoshan Granite in east Shandong Province. Geological Journal of China Universities 3, 1–15 (in Chinese with English abstract).
Zheng, J.P., 1999. Mesozoic–Cenozoic Mantle Replacement and Lithospheric Thinning Beneath the Eastern China. Publishing House of China University of Geosciences, Wuhan. 126 (in Chinese).
Zheng, Y.F., Wang, Z.R., Li, S.G., Zhao, Z.F., 2002. Oxygen isotope equilibrium between eclogite minerals and its constraints on mineral Sm–Nd chronometer. Geochimica et Cosmochimica Acta 66, 625–634.
Zheng, Y.F., Fu, B., Gong, B., Li, H., 2003. Stable isotope geochemistry of ultrahigh pressure metamorphic rocks from the Dabie–Sulu orogen in China: implications for geodynamics and fluid regime. Earth-Science Reviews 62, 105–161.
Zhong, H., Zhu, W.G., Chu, Z.Y., He, D.F., Song, X.Y., 2007. Shrimp U–Pb zircon geochronology, geochemistry, and Nd–Sr isotopic study of contrasting granites in the Emeishan large igneous province, SW China. Chemical Geology 236, 112–133.
Zhou, T.H., Lu, G.X., 2000. Tectonics, granitoids and Mesozoic gold deposits in East Shandong, China. Ore Geology Reviews 16, 71–90.
Zou, H.B., Zindler, A., Xu, X.S., Qi, Q., 2000. Major, trace element, and Nd, Sr and Pb isotope studies of Cenozoic basalts in SE China: mantle sources, regional variations and tectonic significance. Chemical Geology 171, 33–47.
Zhou, J.B., Zheng, Y.F., Zhao, Z.F., 2003. Zircon U–Pb dating on Mesozoic granitoids at Wulian, Shandong Province. Geological Journal of China Universities 9, 185–194 (in Chinese with English abstract).